



KEAP1-NRF2 protein–protein interaction inhibitors: Design, pharmacological properties and therapeutic potential

Enrique Crisman^{1,2,3} | Pablo Duarte^{1,3} | Esteban Dauden³ |
Antonio Cuadrado⁴ | María Isabel Rodríguez-Franco¹  |
Manuela G. López^{2,3} | Rafael León¹ 

¹Instituto de Química Médica, Consejo Superior de Investigaciones Científicas (IQM-CSIC), Madrid, Spain

²Instituto de Investigación Sanitaria La Princesa, Hospital Universitario de la Princesa, Madrid, Spain

³Instituto Teófilo Hernando y Departamento de Farmacología y Terapéutica, Facultad de Medicina, Universidad Autónoma de Madrid, Madrid, Spain

Abstract

The transcription factor nuclear factor erythroid 2-related factor 2 (NRF2) is considered the master regulator of the phase II antioxidant response. It controls a plethora of cytoprotective genes related to oxidative stress, inflammation, and protein homeostasis, among other processes. Activation of these pathways has been described in numerous pathologies

Abbreviations: 2D-FIDA, two-dimensional fluorescence intensity distribution analysis; AD, Alzheimer's disease; ARE, antioxidant response element; BBB, blood–brain barrier; BLI, bio-layer interferometry; BTB, tramtrack, bric-a-brac; BVR, biliverdin reductase; bZIP, cap'n/collar (CNC) basic-region leucine zipper; CAL, calpain cleavage site; CBP, CREB-binding protein; CBR3, carbonyl reductase 3; CD, concentration to double protein expression; CD36, cluster of differentiation 36; CESTA, cellular thermal shift assay; CMA, chaperone-mediated autophagy; COPD, chronic obstructive pulmonary disease; CPP9, cell penetrating-peptide; CRLs, Cullin-RING ligases; CSC, cigarette smoke condensate; CUL1/RBX1, Cullin 1/RING-box protein 1 ubiquitin ligase complex; CUL3, Cullin 3; DMF, dimethyl fumarate; DSF, differential scanning fluorimetry; FITC, fluorescein 5(6)-isothiocyanate; FP, fluorescence polarization; G6PD, glucose 6-phosphate dehydrogenase; GCLc, GCLm, catalytic and modulator subunits of glutamate-cysteine ligase; GPx, glutathione peroxidase; GR, glutathione reductase; GSH, glutathione reduced; GPx, glutathione peroxidase; GSK-3 β , glycogen synthase kinase-3 β ; GSSG, glutathione oxidized; GST, glutathione S-transferase; GSTA3, glutathione S-transferase A3; HO-1, heme-oxygenase-1; IFN γ , interferon production regulator; IFN- γ , interferon gamma; IKK β , inhibitor of kappa light polypeptide gene enhancer in B-cells kinase beta; IL-1 β , interleukin 1 beta; iNOS, inducible nitric oxide synthase; ITC, isothermal titration calorimetry; IVR, intervening region; KEAP1, Kelch-like ECH-associated protein 1; LAMP2, lysosome-associated membrane protein; LPS, lipopolysaccharide; MMF, monomethyl fumarate; MPTP, 1-methyl-4-phenyl-1,2,3,6-tetrahydropyridine; MTCO1, mitochondrially encoded cytochrome C oxidase I; NADPH, nicotinamide adenine dinucleotide phosphate; NASH, nonalcoholic steatohepatitis; Neh, NRF2-ECH homology domains; NF- κ B, nuclear factor- κ B; NLRP3, NOD, LRR-, and pyrin domain-containing protein 3 inflammasome; NO, nitric oxide; NQO1, NAD (P)H:quinone oxidoreductase 1; NRF2, nuclear factor (erythroid-derived 2)-like 2; OCR/ECAR, oxygen consumption and extracellular acidification rate; OSGIN1, oxidative stress-induced growth inhibitor 1; PAMPA, parallel artificial membrane permeability assay; PPI, protein–protein interaction; P-GP, P-glycoprotein 1; RNS, reactive nitrogen species; ROS, reactive oxygen species; SFN, sulforaphane; sMAF, small musculoaponeurotic fibrosarcoma oncogene homologue; SOD, superoxide dismutase; SPR, surface plasmon resonance; SQSTM-1, sequestosome-1; SRXN1, sulfiredoxin 1; STD, saturation transfer difference; TAT, HIV-transactivating transcriptional activator peptide; THIQ, tetrahydroisoquinoline; TNF- α , tumor necrosis factor α ; TR-FRET, time-resolved fluorescence energy transfer; TSA, thermal shift assay; TXNRD1, thioredoxin reductase 1; γ -GCS, γ -glutamylcysteine synthetase; β -TrCP, β -transducin repeat containing protein.

Enrique Crisman and Pablo Duarte contributed equally to this work.

This is an open access article under the terms of the Creative Commons Attribution-NonCommercial-NoDerivs License, which permits use and distribution in any medium, provided the original work is properly cited, the use is non-commercial and no modifications or adaptations are made.

© 2022 The Authors. *Medicinal Research Reviews* published by Wiley Periodicals LLC.

⁴Departamento de Bioquímica, Centro de Investigación Biomédica en Red Sobre Enfermedades Neurodegenerativas (CIBERNED), Instituto de Investigación Sanitaria La Paz (IdiPaz), Instituto de Investigaciones Biomédicas 'Alberto Sols' UAM-CSIC, Facultad de Medicina, Universidad Autónoma de Madrid, Madrid, Spain

Correspondence

Rafael León, Instituto de Química Médica, Consejo Superior de Investigaciones Científicas (IQM-CSIC), C/Juan de la Cierva 3, Madrid 28006, Spain.
Email: rafael.leon@iqm.csic.es

Funding information

Ministerio de Ciencia e Innovación,
Grant/Award Numbers: PID2019-110061RB-I00, PID2021-122650OB-I00, PID2021-123481OB-I00, PID2021-125986OB-I00;
Instituto de Salud Carlos III,
Grant/Award Number: PI17/01700;
Comunidad de Madrid,
Grant/Award Number: B2017/BMD-3827-NRF24ADCM

including cancer, cardiovascular, respiratory, renal, digestive, metabolic, autoimmune, and neurodegenerative diseases. Considering the increasing interest of discovering novel NRF2 activators due to its clinical application, initial efforts were devoted to the development of electrophilic drugs able to induce NRF2 nuclear accumulation by targeting its natural repressor protein Kelch-like ECH-associated protein 1 (KEAP1) through covalent modifications on cysteine residues. However, off-target effects of these drugs prompted the development of an innovative strategy, the search of KEAP1-NRF2 protein-protein interaction (PPI) inhibitors. These innovative activators are proposed to target NRF2 in a more selective way, leading to potentially improved drugs with the application for a variety of diseases that are currently under investigation. In this review, we summarize known KEAP1-NRF2 PPI inhibitors to date and the bases of their design highlighting the most important features of their respective interactions. We also discuss the preclinical pharmacological properties described for the most promising compounds.

KEYWORDS

chronic diseases, KEAP1-NRF2 protein-protein interaction inhibitors, NRF2, NRF2-ARE pathway therapeutic potential, phase II antioxidant response

1 | INTRODUCTION

Nuclear factor-erythroid 2 p45-related factor 2 (NRF2) encoded by *NFE2L2* gene is a transcription factor involved in the control of more than 200 genes that have an enhancer sequence in its promoter region known as the antioxidant response element (ARE).^{1,2} It was discovered in 1994 as a cap'n'collar (CNC) basic-region leucine zipper (bZIP) transcription factor.³ In general, NRF2 participates in the control of several homeostatic functions, such as the antioxidant response, inflammation, and proteostasis, among others.^{2,4} NRF2 is tightly regulated by different mechanisms at transcriptional, epigenetic, or ARE-binding level, however, its key regulation is interceded by proteasome degradation mainly mediated by the repressor protein Kelch-like ECH-associated protein 1 (KEAP1). KEAP1 is an E3 ubiquitin ligase substrate adapter that binds to NRF2 inducing its subsequent ubiquitination by the CUL3/RBX1 complex and degradation by the 26S proteasome.⁵ Indeed, classic electrophilic NRF2 inducers modify Cys residues at KEAP1 leading to conformational changes that induce NRF2 nuclear accumulation.

The broad spectrum of physiological roles regulated by NRF2 suggests that it might be a good target for the development of innovative treatments for different diseases, including neurodegenerative, autoimmune, metabolic, cardiovascular, or cancer.^{6–10} In this sense, its multitarget profile constitutes an important tool to test new approaches for chronic diseases characterized by a complex network of pathological pathways. Among the compounds developed toward this target, dimethyl fumarate (DMF; Tecfidera, Fumaderm, Skilarence) is the first

NRF2 activator in clinical use for the treatment of multiple sclerosis and psoriasis. Many other compounds targeting NRF2 are now under development and several clinical trials are ongoing (i.e., sulforaphane or bardoxolone methyl, among others).⁶

In this review, we discuss in detail a highly innovative type of NRF2 activating compounds: nonelectrophilic noncovalent inhibitors of the KEAP1-NRF2 protein-protein interaction (PPI), which have recently received considerable attention due to their potential advantages. This new class of NRF2 inducers is predicted to enhance the narrow therapeutic window of electrophilic compounds, due to their off-target actions, derived from their promiscuity to react with different types of nucleophiles widely present in many biological molecules.¹¹ For example, the well-known electrophilic triterpenoid CDDO-Im, one of the most potent NRF2 inducers, becomes highly toxic at submicromolar concentrations, probably due to its electrophilic character.¹² The search for PPI inhibitors of the KEAP1-NRF2 axis is a very promising strategy to develop new small molecules that should have fewer side effects than electrophiles. However, further work is required to examine these small molecules for selectivity as disrupters of the NRF2-KEAP1 interaction, pharmacokinetics and toxicological profiles, and protective effects in preclinical models of diseases. At this time, a few PPI inhibitors have been tested for efficacy in animal models of disease, including renal inflammation,¹³ Alzheimer's disease (AD),¹⁴ or lipopolysaccharide (LPS)-induced cardiomyopathy.¹⁵

1.1 | NRF2 physiological functions

NRF2 was known as the antioxidant response master regulator.¹⁶ KEAP1 presents several highly reactive cysteine residues acting as redox state sensors able to promote NRF2 nuclear accumulation after oxidation. Once in the nucleus, NRF2 activates the expression of key enzymes related to the antioxidant response and several metabolic pathways. NRF2 regulates: (i) important enzymes for the production of nicotinamide adenine dinucleotide phosphate (NADPH) redox cofactor, including glucose 6-phosphate dehydrogenase (G6PD, key enzyme for carbohydrate metabolism); (ii) de novo glutathione (GSH) synthetic enzymes, including glutathione S-transferase (GST), glutathione reductase (GR), catalytic (GCLC) and modulator (GCLM) subunits of glutamate-cysteine ligase, γ -glutamylcysteine synthetase (γ -GCS) and glutathione peroxidase (GPx); (iii) key enzymes for the production of antioxidant bilirubin, including heme-oxygenase-1 (HO-1), and biliverdin reductase (BVR); (iv) direct antioxidant enzymes as thioredoxin and (v) NAD(P)H:quinone oxidoreductase 1 (NQO1), an essential enzyme for quinone detoxification.^{6,17-19} In this line, several genes under NRF2 control have been described to promote xenobiotic detoxification, such as *CYP1B1* (cytochrome P450, B1), among others.⁶ Importantly, the liver is considered a first-line defense against food xenobiotics and other oral drugs, as exemplified by work with *Nfe2l2* knockout mice who present exacerbated susceptibility to acetaminophen-induced hepatocellular injury.²⁰

Directly related to the NRF2 phase II antioxidant response regulation is its derived capacity to modulate oxidative stress-mediated inflammation. In this sense, high reactive oxygen species (ROS) levels deregulate the redox systems a pro-inflammatory status which further increases ROS production, resulting in a pathological loop.^{21,22} Additionally, there is a functional cross-talk between NRF2 and the nuclear factor- κ B (NF- κ B) pathway.²³ NF- κ B is a key transcription factor that regulates the inflammatory response in cells and shows multiple connections with NRF2 at different levels. For example, KEAP1 induces the degradation of the inhibitor of Kappa light polypeptide gene enhancer in β -cells Kinase beta (IKK β), resulting in decreased phosphorylation and negative regulation of the NF- κ B pathway.²⁴ Moreover, the *NFE2L2* gene promoter presents several NF- κ B binding sites, indicating that NF- κ B regulates NRF2 expression. Complementarily, there is a competition between NRF2 and NF- κ B-p65 subunit to bind the transcriptional co-activator CBP (CREB-binding protein)-p300 complex, which enhances gene transcription by direct NRF2 or p65 acetylation and potentiates the activation of the antioxidant response or the pro-inflammatory pathway, respectively.^{6,23,25,26} Besides, NRF2 directly regulates the expression of several pro-inflammatory genes by either (i) ARE sequences, that is, the case of CD36 involved in nucleotide

oligomerization domain, leucine-rich repeat-, and pyrin domain-containing protein 3 (NLRP3) inflammasome activation^{6,27} or (ii) by inhibiting RNA polymerase II recruitment for the transcription of different cytokines (i.e., interleukin [IL]-6 and IL-1 β) due to NRF2 binding to the proximity of these genes.²⁸

Considering the clinical implications of aberrant protein deposits in different diseases, especially neurodegenerative disorders, the regulation of protein homeostasis exerted by NRF2 is also a key target activity. Among the autophagy-related genes regulated by NRF2,^{4,6,29} it is noteworthy to mention the transcriptional regulation of the autophagy transporter ubiquitin-binding protein p62, also known as sequestosome-1 (SQSTM1). SQSTM1 is an autophagy cargo receptor protein that recognizes polyubiquitin chains in protein aggregates for selective macroautophagy.^{4,30} Phosphorylated p62 (Pp62) competes with NRF2 to bind KEAP1, inducing KEAP1 degradation via autophagy and, therefore, activating NRF2.³¹ Moreover, NRF2 binding sequences have also been described in the *LAMP2* (lysosome-associated membrane protein) gene, leading to an increase in LAMP2A protein levels upon NRF2 activation.^{29,30} This protein is a lysosomal receptor involved in a selective type of autophagy termed chaperone-mediated autophagy (CMA), where cytosolic proteins carrying the QFERK motif are targeted to the lysosome compartment. One such protein is KEAP1,³² therefore, resulting in a positive feedback loop for NRF2 activation of this autophagy pathway.

The involvement of NRF2 in many cellular pathways it might be a good pharmacological target for the development of innovative treatments for many diseases with different etiology. Its therapeutic potential is evident in view of the large number of ongoing clinical trials with NRF2 activators: bardoxolone methyl is currently in phase III for chronic kidney disease (NCT03749447), autosomal dominant polycystic kidney (NCT03918447), and pulmonary hypertension (NCT03068130); omaveloxolone is in phase II for Friedrich Ataxia (NCT02255435); sulforaphane is in phase II for lung cancer prevention (NCT03232138), and frontal lobe dysfunction (NCT04252261); among others.

2 | STRUCTURAL INSIGHTS AT THE KEAP1-NRF2 AXIS

2.1 | NRF2 regulation: KEAP1 repression and secondary mechanisms

NRF2, encoded by *NFE2L2* gene, is a ubiquitously expressed protein with a rapid turnover (half-life time 15–40 min depending on the cell type).^{6,33} In humans, it presents 605 amino acids, containing seven highly conserved regions known as NRF2-ECH homology (Neh) domains (Neh1–Neh7). The Neh2 domain contains the KEAP1 binding motifs DLG and ETGE, described as the low and high-affinity binding sites for KEAP1, respectively.³⁴ In addition, the Neh6 domain contains two recognition sites for another E3 ubiquitin ligase, the β -transducin repeat containing protein (β -TrCP), a substrate receptor of the Cullin 1/RING-box protein 1 (CUL1/RBX1) ubiquitin ligase complex, which represents an alternative pathway for NRF2 control of protein stability level. Specific phosphorylation of serine residues at DSGIS motif at the Neh6 domain by the glycogen synthase kinase-3 β (GSK-3 β) induces NRF2 recognition by β -TrCP prompting its degradation. β -TrCP also recognizes another motif in the Neh6 domain (DSAPGS) which is constitutively phosphorylated, independently from GSK-3 β activity.³⁵

As previously described, the main regulatory mechanism of NRF2 stability is the control exerted by the repressor protein KEAP1. It belongs to the BTB-Kelch family of proteins, all of which assemble Cullin 3 (herein CUL3) and RBX1 to form multisubunit Cullin-RING (Really Interesting New Gene)-ligases (CRLs) for protein ubiquitination. The BTB-Kelch family comprises around 50 members variously named as Kelch-like 1–42 (KLHL1–42) or Kelch and BTB domain-containing 1–14 (KBTBD1–14). KEAP1 is classified as KLHL19 presenting 611 amino acids (Figure 1).³⁶ Currently, high-resolution structures of full-length KEAP1 high-resolution structures are not available; however, several studies and crystal structures of certain domains have allowed insights into different mechanistic features. KEAP1 protein is composed of three functional domains: (i) broad complex, tramtrack, bric-a-brac (BTB) domain which mediates KEAP1 homodimerization needed for NRF2 recognition and

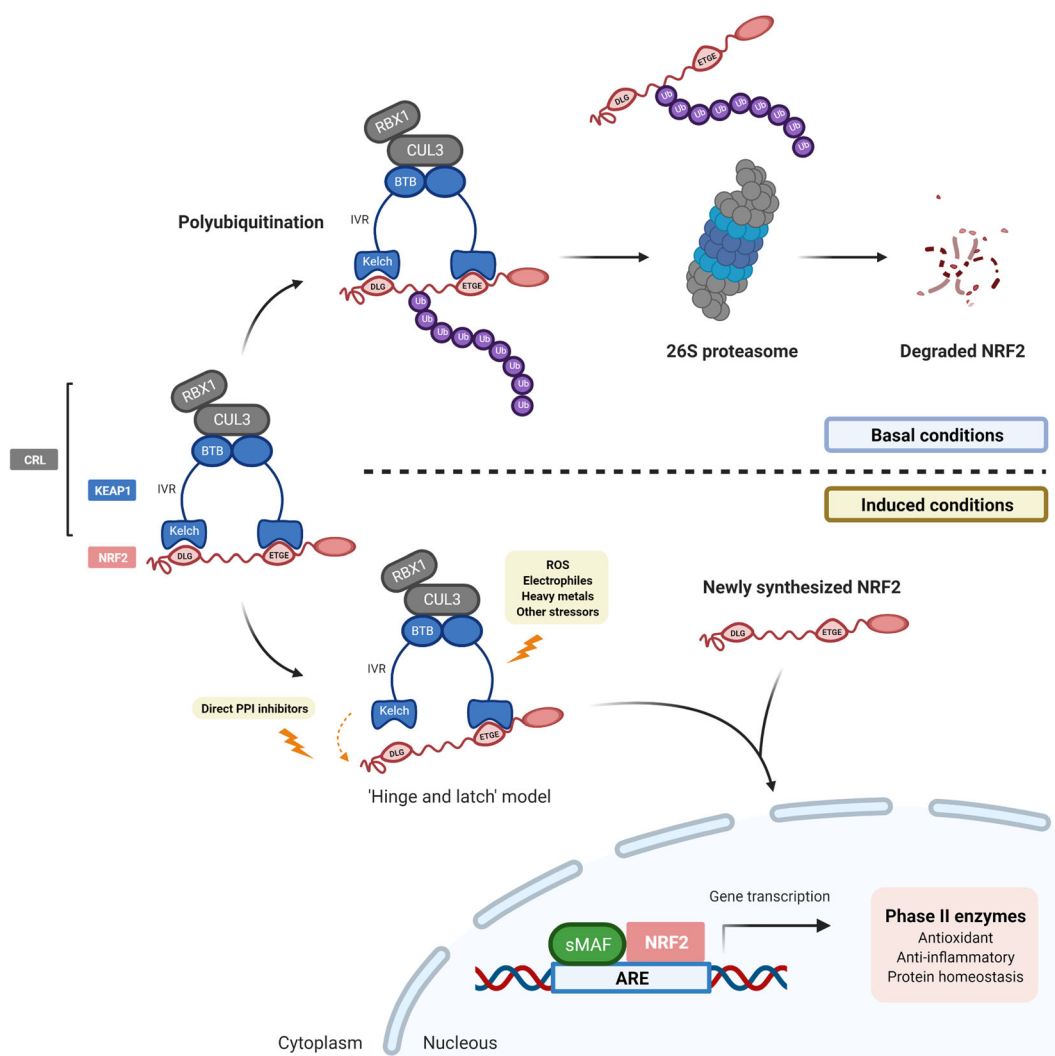


FIGURE 1 Molecular mechanisms of the KEAP1-NRF2 ARE pathway showing the effect of direct protein-protein interaction inhibitors. ARE, antioxidant response element; BTB, bric-a-brac domain; CRL, cullin RING ligases; CUL3, cullin 3; IVR, intervening region; KEAP1, Kelch-like ECH-associated protein 1; NRF2, nuclear factor-erythroid 2 p45-related factor 2; RBX1, RING-box protein 1; ROS, reactive oxygen species; sMAF, small musculoaponeurotic fibrosarcoma oncogene homologue; Ub, ubiquitin. [Color figure can be viewed at wileyonlinelibrary.com]

CUL3 interaction; (ii) the intervening region (IVR) domain, that connects BTB and Kelch domains and contains several important redox sensitive Cys residues; (iii) C-terminal Kelch domain which is responsible for NRF2 binding through the high-affinity ETGE and low-affinity DLG motifs of NRF2 (Figure 1).³⁶ Under basal conditions, NRF2 protein levels are low due to interaction with KEAP1 in the cytoplasm, which targets it for proteasome degradation. Briefly, KEAP1 binds to NRF2 and presents it to the CUL3/RBX1 complex for ubiquitination and subsequent degradation by the 26S proteasome. NRF2 binding to the low and high-affinity motifs (DLG and ETGE, respectively) of the KEAP1 homodimer is mandatory for ubiquitination and proteasomal degradation of NRF2.^{34,36} However, under oxidative stress conditions or in presence of electrophilic compounds, such as some xenobiotics, KEAP1 repressor activity is diminished leading to NRF2 nuclear accumulation. Once in the nucleus, NRF2 dimerizes with

small musculoaponeurotic fibrosarcoma oncogene homologue (sMAF) proteins and this complex binds to the ARE sequences promoting the expression of its target genes (Figure 1).³⁶

KEAP1 contains several highly reactive Cys residues (i.e., Cys151 at the BTB domain, Cys226, Cys273, and Cys288 at the IVR domain, and Cys613 at the Kelch domain) that act as cellular redox status sensors.^{37,38} The relationship of these Cys residues with the activation of the NRF2 pathway has been detailed in the so-called "Hinge and latch model."³⁹ According to this model, Cys residues modification, mainly at the IVR domain, would induce a conformational change that leads to a partial disruption of the interaction between NRF2 and the Kelch domain. NRF2 would remain attached to KEAP1 by the high-affinity interaction at ETGE, however, the low-affinity interaction would be interrupted preventing NRF2 ubiquitination and leading to its accumulation. Thus, the DLG motif could act as a latch to either enable or disable NRF2 degradation, depending on the redox state (Figure 1).^{39,40} In this line, some classical electrophilic NRF2 inducers are known to modify Cys residues at KEAP1, that is, 1-[2-cyano-3,12-dioxooleana-1,9(11)-dien-28-oyl] imidazole (CDDO-Im) and sulforaphane (SFN) target Cys151; 15-deoxy- $\Delta^{12,14}$ -prostaglandin J₂ (15d-PGJ2) targets Cys288. However, these compounds were unable to inhibit the KEAP1-NRF2 interaction.⁴¹ Considering these observations, an alternative hypothesis has been proposed to explain this fact. It has been observed that some compounds reacting with Cys151 are able to block KEAP1-CUL3 interaction, thus, reducing NRF2 ubiquitination. This model known as the "CUL3-dissociation model" would lead to NRF2 saturated KEAP1 making it unable to promote newly synthesized NRF2 ubiquitination and further degradation.^{40,42,43}

Recently, Baird et al.⁴⁴ proposed a new model named as the "conformation cycling model." Under basal conditions, the KEAP1-NRF2 complex would alternate cyclically between an "open state," in which only ETGE motif binds to KEAP1, and a "closed state" in which both ETGE and DLG motifs are bound to KEAP1. Only the "closed state" would allow NRF2 ubiquitination, while the "open state" would offer further regulation. The "conformation cycling model" proposes that Cys modifications at KEAP1 could lead to an abnormal KEAP1-NRF2 interaction "closed state" preventing ubiquitination.⁴⁴ In conclusion, KEAP1 exert multiple mechanisms for NRF2 activation in response to different environmental stresses. All three models indicate that, to activate the phase II antioxidant response, NRF2 is never fully dissociated from KEAP1, thus NRF2 accumulation is related to a combination of KEAP1 function blockade together with de novo NRF2 synthesis.^{41,45}

Additionally, there are other NRF2 activity regulatory mechanisms. At the transcriptional level, NRF2 can be regulated in several manners. In addition to the NF- κ B binding sites located in the *NFE2L2* gene promoter,²³ several oncogenes were shown to increase NRF2 transcription,⁴⁶ such as K-RAS and MYC, with important implications in cancer and tumor development. Moreover, NRF2 is able to bind to its own promoter, since it contains ARE-like sequences,⁴⁷ to increase its own expression. Besides, NRF2 expression can also be suppressed epigenetically by methylation of its promoter as demonstrated in prostate cancer.⁴⁸ As mentioned before, posttranslational modifications of NRF2 protein are known to increase its ARE binding affinity after NRF2-acetylation by the co-activator CBP-p300 complex.²⁶

Considering the high impact of the NRF2 pathway in many physiological processes and its potential use as a therapeutic target in different diseases, a number of compounds are under preclinical and clinical development defined as NRF2 inducers. Regarding its mechanisms, most of them are electrophilic compounds able to react with KEAP1-Cys residues to induce NRF2 nuclear accumulation, as previously described. A prominent example is DMF, approved for the treatment of relapsing-remitting multiple sclerosis. The DMF-derived metabolite, monomethyl fumarate (MMF), readily reacts with Cys151 at the BTB domain of KEAP1 to induce NRF2 pathway activation.^{49,50} Important examples of electrophilic NRF2 inducers are sulforaphane and cyanoenone triterpenoids, that are also under clinical evaluation. Interestingly, cyclic cyanoenes have shown a reversible covalent binding to KEAP1,⁵¹ indicating a slightly different mechanism of action with potential advantages such as the absence of permanent target modification.

It is important to note that, despite that a large number of NRF2 activators have been described in recent years, only a few such as the indicated above, have been included in drug development pipelines that could lead to a

significant therapeutic value. This restraint is due to several factors. First, many of the NRF2 activators are natural products, and as such they cannot be patent protected, reducing the interest for the economical investment that is required for clinical studies. Second, considering that NRF2 is ubiquitously expressed and regulates the expression of a large number of genes, it has been conceptually complicated to define disease-specific and function-specific drugs. However, it should be noted that the NRF2 transcriptional signature is different in specific cells or tissues and also that some drugs display pharmacokinetic properties that are tissue specific. Third, almost all reported activators of NRF2 are electrophilic compounds that participate in sulfhydryl adduct formation with some redox-sensitive Cys residues in several proteins. While the most relevant target of these compounds may be KEAP1, other proteins might be also modified. For example, PTEN is inhibited by tertbutylhydroquinone by adduct formation at cysteine 124 located at its catalytic center.⁵² Another example is the nuclear export of BACH1 by the synthetic triterpenoids CDDO-TFEA and CDDO-Me that are among the most potent NRF2 activators.⁵³ In the case of DMF, part of its anti-inflammatory effect in microglia is NRF2-independent.⁵⁴ Finally, as indicated elsewhere, the current market restraint related to the use of electrophilic compounds is being addressed with a new strategy based on the development of PPI inhibitors of KEAP1-NRF2 (Figure 1). This novel strategy to target so far nondruggable proteins, such as transcription factors, can be also exploited to activate NRF2, however, we still do not know if these nonelectrophilic compounds might have other off-target effects.

In the next sections, we discuss structural details regarding this interaction and summarize all compounds currently developed with this mechanism of action. Although not specifically included in this review, there are other KEAP1-independent NRF2 activators (i.e., compound HPP-4382 as broad complex, tramtrack and BTB and cap'n'collar homology 1 (BACH1) modulator)⁵⁵ and also NRF2 inhibitors for cancer treatment (i.e., compound ML385 interfering with NRF2-sMAF interaction⁵⁶).

2.2 | Structural features of the KEAP1-NRF2 PPI

To date, the KEAP1 and NRF2 full-length structures have not been described, although a complete structural model of the CRL complex can be assembled from its different crystallized subunits (Figure 2A).^{36,58} Nevertheless, KEAP1-Kelch domain complexed with NRF2 peptides containing the ETGE or DLG motifs have been reported revealing the most important structural basis of Neh2 domain recognition by KEAP1 (PDB-ID: 2FLU, 3WN7, 1X2R, 2DYH).^{59–62} The KEAP1-Kelch domain is a six-bladed β -propeller with each blade containing a four-stranded antiparallel β -sheet connected by loops of different length. Loops connecting β -strands A-B and C-D are shorter and exposed to the bottom face of the β -propeller, while longer loops that connect β -strands D-A and B-C extend towards the top face sculpting a shallow pocket for substrate recognition, where NRF2 ETGE and DLG motifs anchor. The binding pocket was divided into six subpockets (P1-P6) based on KEAP1-ETGE (Figure 2B) and KEAP1-DLG (Figure 2C) interactions observed in the cocrystal structures. Subpockets P1 (Arg415, Ile461, Gly462, Phe478, Arg483, Ser508) and P2 (Ser363, Arg380, Asn382, Asn414) are strongly polar, while P4 (Tyr525, Gln530) and P5 (Tyr334, Tyr572, Phe577) have a hydrophobic nature. P3 (Gly509, Ser555, Ala556, Gly571, Ser602, Gly603) is located at the center of the channel formed by small polar residues. P6 (Asp389, Ser431, His432, Gly433, Cys434, Ile435, His436) was identified after cocrystallization of KEAP1 with an extended DLG-containing peptide (DLGex) that displays interactions with these residues at this subpocket⁶⁰ which are not observed for the ETGE motif.

NRF2-ETGE-motif-containing peptides cocrystallized with KEAP1-Kelch domain adopt a β -hairpin conformation within the binding site that comprises residues Asp77, Glu78, Glu79, Thr80, Gly81, and Glu82.^{59,61} This conformation is stabilized by an intramolecular hydrogen bonds network involving backbone atoms of residues Gln75, Asp77, Asp79, Thr80, Glu82, Leu89 and sidechains atoms of residues Asp77 and Thr80. The binding mode is characterized by the interaction of the sidechains of two key glutamate residues with P1 and P2 subpockets. The Glu79 carboxylate is accommodated at P1 subpocket where it establishes critical hydrogen bonds with Arg415 and Arg483 guanidinium moieties and with Ser508 hydroxyl group. Glu82 sidechain is oriented toward the P2

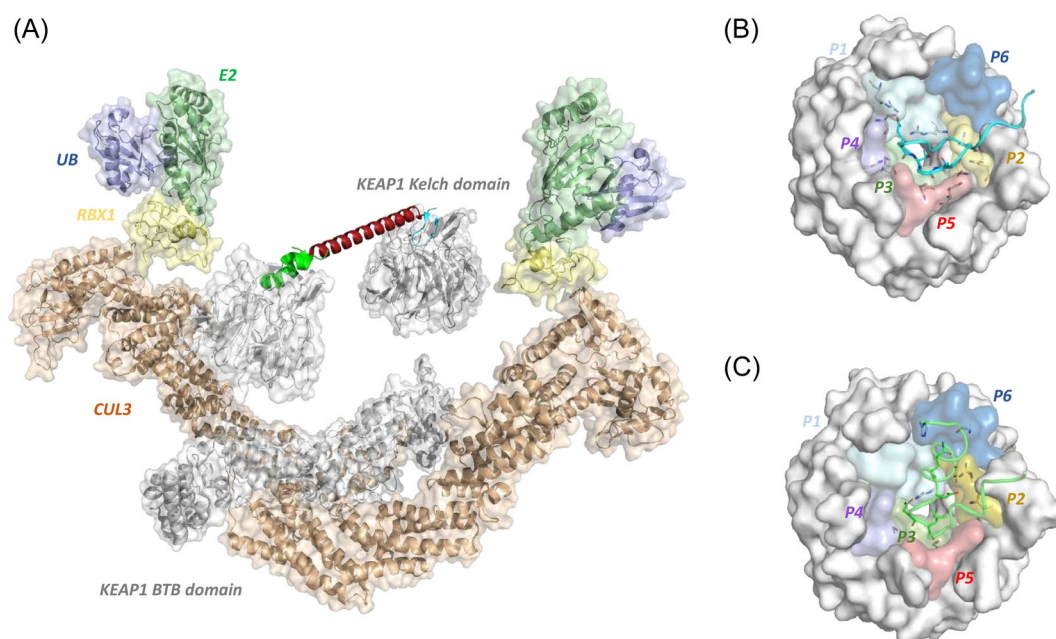


FIGURE 2 Structural basis of KEAP1-NRF2 interaction. (A) Full model of CRL complex as previously described.^{29,47} NRF2 Neh2 domain structure is based on AlphaFold prediction. (B) Binding mode of NRF2 ETGE-containing peptide (PDB-ID 2FLU). (C) Binding mode of NRF2 DLG-containing peptide (PDB-ID 3WN7). BTB, bicauc-a-brac domain; Cul3, cullin 3; E2, ubiquitin-conjugating enzyme E2; RBX1, RING-box protein 1; UB, ubiquitin. Figure was generated with PyMol software.⁵⁷ [Color figure can be viewed at wileyonlinelibrary.com]

subpocket where it interacts with Ser363, Arg380, and Asn382. Additional hydrogen bonds are formed between the ETGE backbone and sidechains of Tyr334, Asn382, Gln530, Ser555, and Ser602, which in combination with several van der Waals contacts and water-bridged interactions, further contribute to the high affinity of KEAP1 for the ETGE motif.

Mouse KEAP1-DLGex complex⁶⁰ revealed that the DLG-containing peptide adopts a U-shape with two short helices (Ile28-Leu30, Arg34-Phe37) and a longer N-terminal helix (Leu19-Arg25) which contrasts with the β -hairpin conformation of the ETGE motif (Figure 3). This spatial conformation is stabilized by electrostatic interactions between Asp18 and Asp21 with Arg34. Despite the conformational differences between ETGE and DLGex peptides overall conformation, their distribution within KEAP1 binding site present similarities as some of the residues involved in the recognition of both motifs partially overlap. However, as can be inferred from the difference in the contact interfaces between KEAP1-ETGE (approximately 529 Å in PDB-ID 1X2R) and KEAP1-DLGex (approximately 820 Å in PDB-ID 3WN7) complexes, there are important differences in their binding mode. DLGex peptide orients the Asp29-sidechain toward P1 subpocket similarly to the ETGE peptide Glu79. However, Asp29-sidechain does not insert as deeply in P1 and, therefore, the extensive hydrogen bond network observed for the ETGE motif is not reproduced. Instead, Asp29 carboxyl group forms a strong salt bridge exclusively with KEAP1-Arg415. Asp27 sidechain interacts with Arg380, Asn382, and Asn414 at P2 subpocket. Interaction at P2 is strengthened via hydrogen bonding between Gln26 and Arg380 sidechains. Similarly to the ETGE motif, several DLGex backbone atoms interact with KEAP1 residues. Specifically, Leu23, Arg25, Gln26, Asp29, and Leu30 carbonyl groups act as hydrogen bond acceptors of KEAP1 residues Arg380, Arg415, Arg483, Ser555, and Ser602. Another difference concerns the interaction of DLGex with residues belonging to the P6 subpocket by means of the hydrogen bonds that Gln26 establishes with the imidazole group of His436 and the carbonyl group of Gly433, interactions that are

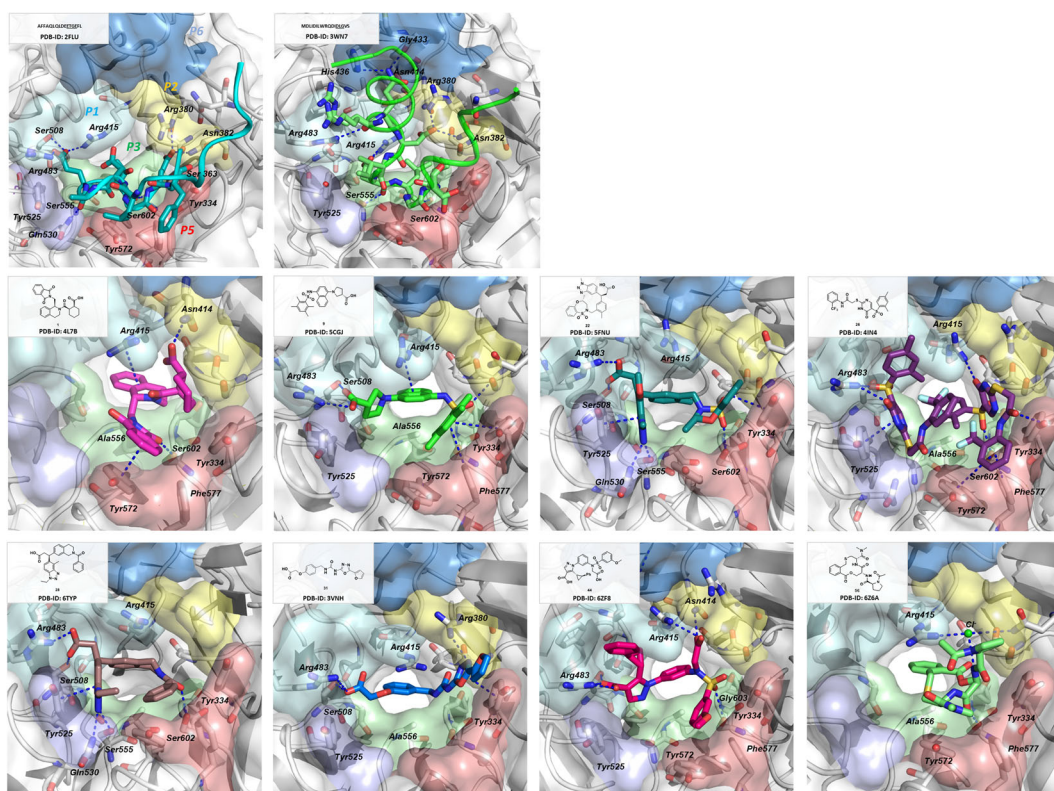


FIGURE 3 X-ray crystallographic structures of KEAP1-NRF2 ETGE and DLG truncated peptides (top row) and KEAP1 complexed with several compounds discussed in this review. Figure was generated with PyMol software.⁵⁷ [Color figure can be viewed at wileyonlinelibrary.com]

not observed for the ETGE peptide. Overall, the differences in the binding mode of both peptides reflect their distinct binding thermodynamics and kinetics profile.

3 | KEAP1-NRF2 PPI INHIBITORS: DESIGN AND PHARMACOLOGY

Several peptides and small molecules have been described in recent years as KEAP1-NRF2 PPI inhibitors, as discussed in the following sections. Extensive reviews about these privileged scaffolds have been previously published.^{45,63–65} Here, we focused on the pharmacological profile and preclinical studies with the known KEAP1-NRF2 PPI inhibitors targeting several diseases.

3.1 | Peptides

Targeting PPI interfaces is considered one of the main challenges in drug discovery. The large (~1500–3000 Å²) and usually shallow topology of PPIs contact hampers the design of small molecule-based drugs,^{66,67} thus, initial efforts were devoted to obtain small peptides that represent an attractive strategy for targeting PPI sites, given their capability of mimicking the natural-occurring interactions, their easy synthesis and modification and the possibility of basing their design on the natural protein.^{66,68} Furthermore, peptide PPI modulators have traditionally helped in

the identification of “hot spots,” that is, well-defined sites that drive molecular binding, which constitute a critical element in the design of additional peptide or small-molecule modulators. Thus, peptide-based targeting of PPI interfaces is usually used as the first approach in PPI modulator development. Fortunately, KEAP1-NRF2 interface constitutes an exception among PPIs given their area of contact, which resembles those of small molecule–protein interactions (~300–1000 Å²).

3.1.1 | Minimal NRF2 sequence for KEAP1 interaction

Initial studies considering peptides as PPI inhibitors were focused on determining the minimal ETGE-containing peptide sequence required for KEAP1 binding. Lo et al.⁵⁹ revealed that 16-mer (**p1**), 14-mer (**p2**), and 10-mer (**p3**) ETGE-containing NRF2-derived peptides (Table 1) were able to displace NRF2 from KEAP1 binding in a pull-down assay. Following this work, Hu's group synthesized a novel series of ETGE-containing peptides of different lengths as potential KEAP1 ligands able to interrupt KEAP1-NRF2 complex.^{69,72} From these studies, 9-mer peptide **p8** (Table 1) was identified as the minimal NRF2 sequence able to bind KEAP1 ($K_{d, \text{binding (SPR)}} = 352 \text{ nM}$) as KEAP1 affinity drastically diminished ($K_{d \text{ (SPR)}} > 1 \mu\text{M}$) for 8mer (**p12**) and 7mer (**p14**) peptides (Table 1).⁷² Besides, **p8** N-terminus acetylation led to an important affinity potentiation (**p10**; $K_{d \text{ (SPR)}} = 23.1 \text{ nM}$; Supporting Information: Table S1) showing similar potency to the longer 16-mer peptide (**p1**; $K_{d \text{ (SPR)}} = 23.9 \text{ nM}$). These results were in agreement with those obtained in fluorescence polarization (FP) and surface plasmon resonance (SPR) assays of fluorescein isothiocyanate (FITC)-labeled ETGE-containing peptides.⁶⁹ FITC-9-mer peptide **p20** displayed notably higher affinity for KEAP1 ($K_{d \text{ (FP)}} = 65.1 \text{ nM}$, $K_{d \text{ (SPR)}} = 33.2 \text{ nM}$, Supporting Information: Table S1) than the shorter FITC-8-mer peptide **p22** ($K_{d \text{ (FP)}} \sim 750 \text{ nM}$, $K_{d \text{ (SPR)}} \sim 835 \text{ nM}$, Supporting Information: Table S1). Congruently, the 9mer peptides **p8** and its N-acetylated derivative **p10** inhibited KEAP1-NRF2 interaction in a FP assay ($\text{IC}_{50 \text{ (FP)}} = 3.48 \mu\text{M}$ and $\text{IC}_{50 \text{ (FP)}} = 194 \text{ nM}$, respectively). However, the authors observed that the 8-mer peptide **p12** was also able to disrupt KEAP1-NRF2 interaction ($\text{IC}_{50 \text{ (FP)}} = 21.7 \mu\text{M}$), suggesting that indeed this was the shortest peptide with PPI inhibitory activity.⁶⁹

Interestingly, Hancock et al. reported a different conclusion when evaluating the KEAP1-NRF2 inhibitory potency of ETGE-containing peptides by an FP assay.⁷⁰ Results from Hancock et al. demonstrated that 7-mer peptide **p24**, Table 1 inhibited KEAP1-NRF2 interaction ($\text{IC}_{50 \text{ (FP)}} = 5.39 \mu\text{M}$). Explanation of differences can be found at a structural level, 7-mer peptide developed by Hu et al. (**p14**) lacked Asp77, which seems to stabilize the β -hairpin conformation of the peptide by the establishment of intramolecular hydrogen bonds. Depletion of Asp77 or Phe83 led to inactive peptides, thus indicating that indeed **p24** is the shortest ETGE-containing peptide with NRF2 displacing capability.

3.1.2 | ETGE, DLG, and p62-derived peptides

Hancock and coworkers⁷⁰ explored the effect of residue substitutions in peptide **p24** (Table 1). They found that replacement of Glu78 by Ala led to a notable increase in potency (**p29**; $\text{IC}_{50 \text{ (FP)}} = 730 \text{ nM}$, Table 1), however, additional modifications at any other residue were detrimental for activity (**p26**–**p39**, Supporting Information: Table S1) except in the case of Phe83Trp (**p37**; $\text{IC}_{50 \text{ (FP)}} = 558 \text{ nM}$). The authors also conducted a mutagenesis study on the 7-mer DLG-derived peptide **p43** (Table 1) in which it was demonstrated that the native DLG sequence showed the highest potency among all peptides (**p44**–**p54**, Supporting Information: Table S1). Additionally, modifications of a 7-mer peptide based on sequestosome-1 binding motif **p55** ($\text{IC}_{50 \text{ (FP)}} = 34.4 \mu\text{M}$, Table 1) led to the identification peptide **p56**, by substitution of Ser by Glu residue, with increased inhibitory potency ($\text{IC}_{50 \text{ (FP)}} = 115 \text{ nM}$, Table 1). **P56** can be considered an ETGE-derived peptide in which the first Glu residue has been substituted by Pro, which leads to a dramatic potency improvement (**p57** vs. **p24**), presumably by stabilizing

TABLE 1 Described peptide KEAP1-NRF2 PPI inhibitors

Peptide sequence		Biological activity	References
<i>ETGE, DLG, and p62-derived peptides</i>			
p1	H-AFFAQLQLDEETGEFL-OH	K_d (ITC) = 20 nM K_d (SPR) = 23.9 nM IC_{50} (FP) = 0.163 μ M PDB-ID 2FLU	[48, 55, 56]
p2	H-LQLDEETGEFLPIQ-OH	KEAP1 binding (pull-down assay)	[48]
p3	H-LDEETGEFLP-OH	KEAP1 binding (pull-down assay)	[48]
p8	H-LDEETGEFL-OH	K_d (SPR) = 352 nM IC_{50} (FP) = 3.48 μ M	[55, 56]
p12	H-DEETGEFL-OH	K_d , (SPR) > 1000 nM IC_{50} (FP) = 21.7 μ M	[55, 56]
p14	H-EETGEFL-OH	K_d , (SPR) > 1000 nM IC_{50} (FP) > 100 μ M	[55, 56]
p24	Ac-DEETGEF-OH	IC_{50} (FP) = 5.39 μ M ΔTm = 1.95°C	[58]
p29	Ac-D <u>A</u> ETGEF-OH	IC_{50} (FP) = 730 nM	[58]
p43	Ac-WRQDIDL-OH	IC_{50} (FP) = 17.1 μ M	[58]
p55	Ac-D <u>P</u> <u>S</u> T <u>G</u> E <u>L</u> -OH (Sequestosome-1)	IC_{50} (FP) = 34.4 μ M	[58]
p56	Ac-D <u>P</u> <u>E</u> T <u>G</u> E <u>L</u> -OH	IC_{50} (FP) = 0.115 μ M K_d binding (ITC) = 0.25 μ M ΔG = -9.03 kcal/mol; ΔH = -9.07 kcal/mol; $T\Delta S$ = -0.03 kcal/mol Functional cell assays: NQO1 induction assay	[58]
p57	Ac-D <u>P</u> <u>E</u> T <u>G</u> E <u>F</u> -OH	IC_{50} (FP) = 0.248 μ M	[58]
p68	St-D <u>P</u> <u>E</u> T <u>G</u> E <u>L</u> -OH	IC_{50} (FP) = 0.022 μ M Functional cell assays: NQO1 induction assay	[60]
p80	Ac-D <u>P</u> <u>E</u> T <u>G</u> E(<u>Cha</u>)-OH	IC_{50} (FP) = 85 nM K_d (ITC) = 0.075 μ M ΔG = -9.57 kcal/mol; ΔH = -9.83 kcal/mol; $T\Delta S$ = -0.29 kcal/mol ΔTm = 5.8°C	[61]
p84	Ac-D(<u>Thp</u>)ET <u>G</u> E <u>L</u> -OH	IC_{50} (FP) = 89 nM K_d (ITC) = 0.31 μ M ΔG = -8.95 kcal/mol; ΔH = -12.83 kcal/mol; $T\Delta S$ = -3.84 kcal/mol ΔTm = 8.3°C	[61]

(Continues)

TABLE 1 (Continued)

	Peptide sequence	Biological activity	References
p86	Ac-D(Thp)ETGE(Cha)-OH	IC ₅₀ (FP) = 31 nM K _d (ITC) = 0.056 μM ΔG = -9.89 kcal/mol; ΔH = -23.2 kcal/mol; TΔS = -13.25 kcal/mol	[61]
p87	Ac-LDPETGEFL-OH	K _d (ITC) = 46.5 nM ΔG = -10.0 kcal/mol; ΔH = -10.9 kcal/mol; TΔS = -0.9 kcal/mol K _d (BLI) = 65.3 nM IC ₅₀ (FP) = 42.6 nM	[59]
p88	Ac-LDPETGEYL-OH	K _d (ITC) = 42 nM ΔG = -10.1 kcal/mol; ΔH = -17.8 kcal/mol; TΔS = -7.7 kcal/mol K _d (BLI) = 16.6 nM IC ₅₀ (FP) = 29.6 nM	[59]
<i>Cycle and CPP-conjugated peptides</i>			
p183	Ac-c[CLDPETGEYLC]-OH	K _d (ITC) = 10.4 nM ΔG = -10.9 kcal/mol; ΔH = -13.1 kcal/mol; TΔS = -2.2 kcal/mol K _d (BLI) = 2.8 nM IC ₅₀ (FP) = 9.45 nM	[59]
p187	c[GQLDPETGEFL]	K _d (ITC) = 18.12 nM K _d (BLI) = 6.19 nM IC ₅₀ (FP) = 18.31 nM IC ₅₀ (FP) = 19 nM Functional cell assays: ARE-luciferase reporter assay NRF2-dependent response, antioxidant and anti-inflammatory in LPS-stimulated RAW 264.7 cells	[63, 64]
p189	CPP9-c[GQLDPETGEFL]	IC ₅₀ (FP) = 153 nM Metabolic stability in human serum	[64]
p211	H-YGRKKRRQRRR- LQLDEETGEFLPIQ-NH ₂	Functional cell assays: NRF2-dependent response, anti-inflammatory effect in LPS-stimulated THP-1 cells	[67]
p212	O2beY-DSETGE-C	K _d (FLAG-tagged peptide washing) = 110 nM, IC ₅₀ (FLAG-tagged peptide washing) = 2.8 nM	[68]
p214	O2beY-DVETGE-C	K _d (FLAG-tagged peptide washing) = 425 nM	[68]

TABLE 1 (Continued)

	Peptide sequence	Biological activity	References
<i>Other peptides</i>			
p222	Ac-EWWW-OH	K_d (SPR) = 77 μ M K_d (ITC) = 10 μ M ΔG = -7.0 kcal/mol; ΔH = -3.8 kcal/mol; $T\Delta S$ = -3.1 kcal/mol IC_{50} (TR-FRET) = 30 μ M Cocrystal structure (PDB-ID: 5 \times 54)	[69]
<i>Peptides with in vivo studies</i>			
p223	H-YGRKKRRQRRR-PLFAER-LDEETGEFLP-NH ₂ ; TAT-CAL-10mer	In vivo mouse model of traumatic brain injury	[70]
p224	H-RKKRRQRRR-PLFAER-LDEETGEFLP-NH ₂ ; TAT-CAL-10mer	In vivo rat model of global cerebral ischemia	[71]

Abbreviations: BLI, biolayer interferometry assay; FP, fluorescence polarization; ITC, isothermal titration calorimetry; KEAP1, Kelch-like ECH-associated protein 1; LPS, lipopolysaccharide; NADPH, nicotinamide adenine dinucleotide phosphate; NQO1, NAD(P)H:quinone oxidoreductase 1; NRF2, nuclear factor erythroid 2-related factor 2; SPR, surface plasmon resonance; TR-FRET, time-resolved fluorescence resonance energy transfer.

the β -hairpin conformation, which translates into a reduced entropy loss upon binding,⁷¹ and a substitution of the terminal Phe by Leu, which slightly improves potency (**p56** vs. **p57**). Aminoacidic substitutions in **p56** sequence by Hancock et al. failed to yield an improvement in activity (**p57**-**p67**, Supporting Information: Table S1),^{70,73} Further evaluation of **p56** led to the introduction of an N-terminal C18 fatty acid stearic acid to obtain peptide **p68**,⁷³ which showed a fivefold potency increase (IC_{50} (FP) = 22 nM, Table 1). Peptide **p68** exhibited a modest CD (concentration to double protein expression) value of 50–80 μ M to induce NQO1 expression in Hepa1c7 cells, while parental peptide **p56** exhibited no cell activity due to its low cell permeability. Additional N and C-terminal capping groups were explored (**p69**-**p77**, Table S1) without any activity improvement.^{73,74} Effect of nonnatural amino acids introduction in peptide **p56** sequence (**p78**-**p86**, Table S1)⁷⁴ led to the improved peptides **p80** (IC_{50} (FP) = 85 nM, Table 1) and **p84** (IC_{50} (FP) = 89 nM, Table 1), presumably due to the establishment of stronger interactions with P5 and P1 subpockets respectively. Combination of **p80** and **p84** led to **p86**, which exhibited the highest potency among all evaluated peptides (IC_{50} (FP) = 31 nM, Table 1).

Modification of peptide **p56** by Lu et al.⁷¹ by incorporation of an N-terminal Leu and C-terminal aromatic residues Phe or Tyr led to peptides **p87** and **p88**, which exhibited an improvement in its inhibitory potency (IC_{50} (FP) = 42.6 nM and 29.6 nM, respectively, Table 1), presumably due to the establishment of stronger interactions with P4 and P5 subpockets.

Recently, Colarusso et al.⁷⁵ explored the effect of several modifications on residues Glu78, Glu79, Thr80, and Glu82 of peptide **p11** (**p126**-**p182**, Supporting Information: Table S1). Glu78, Glu79, and Glu82 were targeted to reduce the acidic nature of the peptide and increase their cell permeability, while Thr80 replacement was oriented to explore P3 subpocket binding. Among natural amino acids, the substitution of Glu78 by Pro led to the most drastic increase in potency measured by time-resolved fluorescence resonance energy transfer (TR-FRET) (**p95**, IC_{50} (TR-FRET) = 19 nM, Supporting Information: Table S1). Evaluation of nonnatural proline analogs revealed several interesting conclusions: substitutions at position 4 of the pyrrolidine ring were well tolerated, independently of the nature of the substituent. Indeed, peptide **p96** and **p97** (IC_{50} (TR-FRET) = 13 nM and IC_{50} (TR-FRET) = 11.8 nM, respectively, Supporting Information: Table S1), bearing one or two fluorine atoms in that position, had a nearly

twofold potency increase compared to the natural proline. On the other hand, substitutions on positions 3 or 5 were detrimental, presumably by destabilizing the β -turn conformation of the peptide. Substitution of the pyrrolidine by a thiazolidine ring yielded a twofold gain in potency (**p117**, Supporting Information: Table S1). Other modifications of the nature of the pyrrolidine ring, such as the introduction of an additional carbon (homoproline) or inversion of the configuration of the alpha carbon, resulted in a critical loss of potency. Based on **p97** peptide, replacement of Thr80 was then evaluated in which removal of the hydroxyl or methyl groups of the Thr80 sidechain was detrimental for activity. Similarly, the substitution of the methyl moiety by more voluminous groups also led to decreased potency. Based on the cocrystal structure of peptide **p95** and KEAP1 (PDB-ID **6T7V**), this effect was attributed to the Glu79-Arg415 interaction, which causes Arg415 to adopt an orientation that leads to a blockade of the P3 subpocket. By introducing mutation Glu79Gly to avoid the electrostatic interaction with Arg415, it was demonstrated that substitution of the Thr80 methyl group by larger moieties led to an increase of potency, presumably due to the accessibility to P3 subpocket, in good agreement with the starting hypothesis. Substitution of the Glu79 or Glu82 residues led to drastic decrease in potency. However, none of the reported linear peptides were active in cell-based assays.

3.1.3 | Cycled and CPP-conjugated peptides

Since β -hairpin conformation is critical for ETGE-derived peptide binding efficacy, Lu and coworkers⁷¹ considered cyclization as a promising strategy to improve their affinity as it could lock peptides in their bioactive conformation, avoiding entropy loss upon binding. Moreover, peptide cyclization has shown other advantages such as protease-cleavage resistance and improved membrane permeability.⁷⁶ Thus, the addition of a terminal disulfide-bond to **p88** led to peptide **p183**, which showed a threefold potency improvement as PPI inhibitor ($IC_{50 (FP)} = 9.45$ nM) and a fourfold higher affinity for KEAP1 as measured by isothermal titration calorimetry (ITC) ($K_d, \text{binding (ITC)} = 10.4$ nM). Authors also reported head-to-tail cycled peptide **p187** (Table 1), being N-terminal glycine included a flexible linker to avoid loss of bioactive conformation upon cycling.⁷⁶ **p130** showed a 3.5-fold increased potency to inhibit KEAP1-NRF2 ($IC_{50 (FP)} = 18.31$ nM) compared to the corresponding linear peptide **p188** (Supporting Information: Table S1) and 4.5-fold increase in KEAP1 affinity ($K_d, \text{binding (ITC)} = 18.12$ nM, $K_d, \text{binding (BLI)} = 6.19$ nM). More interestingly, **p187** was able to increase luciferase activity in the HepG2-ARE-C8 cells (3.4-fold at 1 μ M) and to induce NRF2 nuclear localization and NRF2-downstream genes expression in RAW264.7 cells, providing anti-inflammatory and antioxidant effects. However, **p187** permeability was relatively poor due to its high polarity. **p187** cell permeability was improved by conjugation with a high-efficiency cytosolic delivery cell penetrating-peptide (CPP9) via a poly-ethylene glycol-lysine linker.⁷⁷ The resulting peptide **p189** (Supporting Information: Table S1) exhibited an exclusive cytoplasmatic localization and a 98-fold improved penetration compared to **p187**. Conversely, CPP9-conjugation reduced its KEAP1-NRF2 PPI inhibitory potency ($IC_{50 (FP)} = 153$ nM). Despite its lower affinity, **p189** enhanced cell permeability resulted in an increased Nrf2 induction potency in the ARE-HepG2 cell line (**p187** $EC_{50} > 10$ μ M, **p189** $EC_{50} = 1.1$ μ M), and increased NRF2 and HO-1 protein levels in HEK293T cells.

Steel and coworkers⁷⁸ reported different disulfide bond-based cyclic peptides (**p190–194**) and perfluoroaryl-bridged peptides (**p195–p198**, Supporting Information: Table S1), which showed increased potency in relation to their linear counterparts (**p199–p201**, Supporting Information: Table S1). However, none of them were active in cell-based assays. Chen et al.⁷⁹ demonstrated that the increase in KEAP1 affinity by a disulfide bond-based cycling strategy also applies to DLG and longer ETGE peptides, with 7.5- and 3.5-fold increases in binding affinity for peptides **p202** and **p205** compared to their linear analogues (**p204** and **p207**, Supporting Information: Table S1).

Colarusso et al.⁷⁵ also used cyclization as a strategy to improve cell activity, based on the sequence of peptide **p96** (Supporting Information: Table S1). They explored several cyclization strategies, including head-to-tail, disulfide bonds, side chain to side chain lactam bridges, side chain to tail lactam bridges, hydrocarbon linker, and triazol linker. Some of the resulting peptides exhibited high potency as PPI inhibitors, that is, **p209** ($IC_{50} = 11$ nM, Supporting

Information: Table S1) and **p210** (IC_{50} = 16 nM, Supporting Information: Table S1), however, none of the cyclizing strategies led to a cell-active peptide. Additional conjugation with CPPs was neither able to provide cell activity.

Steel et al.⁸⁰ reported an innovative strategy in which 14-mer ETGE-containing peptide was conjugated with the HIV-transactivating transcriptional activator peptide (TAT), (**p211**, Table 1). Peptide **p211** increased NRF2 protein levels together with HO-1 mRNA and protein levels in the human monocyte cell line THP-1. Moreover, **p211** preincubation of THP-1 cells reduced TNF- α mRNA levels after LPS treatment.

Recently, Owens et al.⁸¹ reported a series of cyclized peptides with sequences O2beY-XXEXGE-C, O2beY-XEEXXE-C, O2beY-DXEXGE-C, C-XXEXGE-O2beY, C-XEEXXE-O2beY, and C-DXEXXE-O2beY. O2beY represents O-(2-bromoethyl)-tyrosine, which allows peptide-cyclization by nucleophilic attack to the terminal cysteine, and X represents any residue. Combined, the resulting libraries contained 5×10^4 different peptides. After four rounds of affinity selection, the authors found that two families of peptides, with the consensus sequences O2beY-D(S/T)ETGE-C and O2beY-D(Φ)E(T/S)GE-C, were the most active. Peptides **p212** (O2beY-DSETGE-C) and **p2214** (O2beY-DVETGE-C), selected as representatives of each family, exhibited high affinity for KEAP1 (K_d = 110 nM and 425 nM, respectively, Table 1). Cyclization showed to be critical for binding as **p212**-derived linear peptide **p214** (Supporting Information: Table S1) had a fivefold lower KEAP1 affinity. **p212** was able to compete with NRF2 for KEAP1 binding in a FLAG-tagged peptide washing-based assay (IC_{50} = 2.8 nM). The authors also explored a more randomized library with sequence O2beY-(X)₆-C, which included approximately 10^8 different peptides. After three rounds of affinity selection, all hit peptides were tested in vitro identifying peptides **p215**–**p216** (Supporting Information: Table S1). It is interesting to note that, despite the random nature of the strategy followed, the highest affinity peptides **p215** and **p216** included the ETGE motif in their sequence. **p217**–**p219** exhibit a completely different sequence compared to previously reported peptides, although with lower affinities. Among them, **p217** is especially intriguing given the lack of negatively charged amino acids in its sequence.

3.1.4 | Other peptides

Li et al. reported two egg-derived tripeptides **p220** and **p221** (Supporting Information: Table S1), that were able to disrupt KEAP1-NRF2 interaction in an FP assay and exert a protective effect in HEPG2 cells upon H₂O₂ induced toxicity at a 10 and 100 μ M concentration.⁸² By means of a phage-display peptide screening strategy, Sogabe et al.⁸³ identified tetrapeptide **p222** (Table 1) which was able to bind to KEAP1 (K_d (SPR) = 77 μ M, K_d (ITC) = 10 μ M) and inhibit KEAP1-NRF2 interaction (IC_{50} (TR-FRET) = 30 μ M). The crystallographic structure of the KEAP1-**p222** complex (PDB-ID 5 \times 54) shows that the peptide places its terminal and Glu carboxylic acids in a similar position to Glu82 and Glu79 of ETGE-peptides, respectively. Nonetheless, **p222** terminal Trp is inserted at the central cavity, establishing a cation- π interaction with KEAP1-Arg415, which is a common feature of many reported small molecule inhibitors, while Trp3 establishes a π - π interaction with Tyr525.

3.1.5 | In vivo studies with peptides

Further evaluation of fusion-peptides to test their potential drug-like properties in vivo led to the development of peptide **p223** (Table 1).⁸⁴ **p223** contains the HIV-TAT followed by the calpain cleavage site (CAL) and an ETGE containing peptide allowing injury-specific liberation of **p223**. In a mouse model of traumatic brain injury, **p223** increased mRNA levels of several NRF2-downstream genes in the parietal cortex. Furthermore, **p223** treatment reduced blood-brain barrier (BBB) permeability caused by traumatic brain injury after intracerebroventricular administration 2 h before injury and also after intrathecal administration 10 min postinjury, thus demonstrating the therapeutic potential of KEAP1-NRF2 PPI inhibition in an in vivo model for the first time. Thereafter, Tu et al.⁸⁵ demonstrated the therapeutic effect of an equivalent TAT-CAL-DEETGE peptide (**p224**, Table 1) in a rat model of

global cerebral ischemia. **p224** pretreatment via intraventricular administration led to an injury-specific NRF2 nuclear translocation and NRF2-driven genes expression at the CA1 hippocampal region. Activation of the phase II response significantly reduced oxidative stress injury resulting in an important neuroprotective effect and, more importantly, it promoted significant cognitive function preservation. Encouraged by these observations, the authors explored the protective potential of post-injury peripheral treatment. **p224** was administered subcutaneously 1 day after GCI injury and maintained until the conclusion of the experiment (9 days). Similarly to intracerebral administration, neuroprotection, and cognitive loss prevention were achieved, thus demonstrating that KEAP1-NRF2 PPI inhibition can be a promising therapeutic strategy for the treatment of global cerebral ischemia.

3.2 | Small molecules

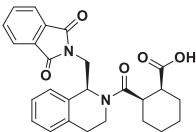
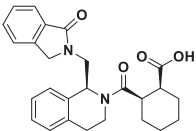
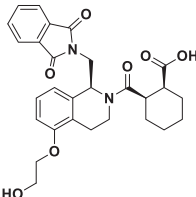
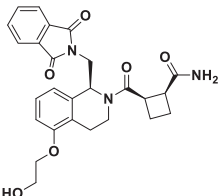
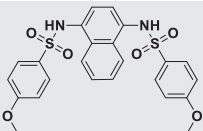
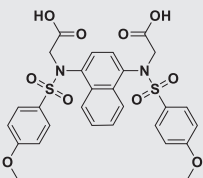
3.2.1 | 1,2,3,4-Tetrahydroisoquinoline compounds

As previously introduced, peptides were the first noncovalent KEAP1-NRF2 PPI inhibitors, however, they offered some disadvantages related to their membrane permeability limiting their cellular activity. Hu et al.⁸⁶ reported the first small compound as a direct KEAP1-NRF2 PPI inhibitor, belonging to the tetrahydroisoquinoline (THIQ) class of compounds. Using fluorescein-labeled 9mer NRF2 peptide amide as the fluorescent probe and KEAP1 Kelch domain as the target protein, 337,116 compounds from the NIH's Molecular Libraries Probe Production Centers Network library were screened. The most promising hit from this high throughput screening (HTS) showed an IC_{50} value in the FP assay of 3 μ M and the binding constant (K_d) to the KEAP1 Kelch domain of 1.9 μ M using an SPR competition assay. This hit was a mix of four stereoisomers, thus, after an enantioselective synthesis, they obtained compound **1** (named as **LH601A** or probe **ML334**, Table 2) as the most active diastereoisomer (*S,R,S*-configuration) being 100-fold more potent than its diastereoisomers (K_d = 1.0 μ M towards KEAP1 in the SPR assay). Compound **1** was shown to be active in different functional cell assays: (i) EC_{50} of 18 μ M in CellSensor ARE-bla HepG2 cell line and; (ii) EC_{50} = 12 μ M for NRF2 nuclear translocation evaluated in PathHunter U2OS KEAP1-NRF2 functional assay. Additionally, compound **1** showed reversible KEAP1-NRF2 interaction inhibition and no adduct formation after incubation with GSH demonstrating its lack of electrophilicity. Continuing this line of research, different series of analogues were evaluated for initial structure-activity relationships (SAR) all of them leading to a reduced SPR assay activity compared to **1**.^{86,87} Interestingly, compound **1** induced NRF2 target genes upregulation (*HO-1*, *TRX1*, and *NQO1*) and increased protein levels (*HO-1* and *TRX1*) in human embryonic kidney cells (HEK293) demonstrating its capacity to cross the cellular membrane to exert its KEAP1-NRF2 PPI inhibitory activity.⁸⁸

Jnoff et al.⁸⁹ (UCB Pharma and Evotec) reported the cocrystal structure of **1** with KEAP1 Kelch domain (PDB-ID **4L7B**) showing the aromatic ring of the THIQ group allocated into the central pore and important interactions between carboxylic acid and both Arg380 and Arg415. Based on this information, new analogues of compound **1** were synthesized and evaluated in FP assay (compounds **1a-h** and **2a-2c** for SAR, Supporting Information: Table S2). Among them, only few showed a slightly improved potency, exemplified by most potent compound **2** (Table 2), stating that few structural modifications of structural core of **1** are allowed considering activity. Cocrystal structures with KEAP1 Kelch domain were also reported for several derivatives including compound **2** (PDB-ID **4L7D**, Table 2 and Supporting Information: Table S2). To further characterize their pharmacological properties, authors measured efflux ratio (ER) in MDCK-MDR1 cells and assessed in vivo brain exposure. Compound **1** showed a high ER (= 20) and a small unbound brain-to-plasma ratio (B_u/P_u < 0.01) in mice. Additional experiments with *Mdr1a/1b/Bcrp* knockout mice showed an improved ratio (B_u/P_u = 0.4) confirming that compound **1** is a P-glycoprotein 1 (P-GP) substrate. Carboxylic acid moiety removal greatly improved in brain exposure, however, this modification resulted in loss of activity in the FP assay (structure and data not shown).⁸⁹

Ontoria et al.⁹⁰ developed new series of THIQ compounds in which the carboxylic acid moiety was replaced by primary amides trying to improve their permeability. They used compound **1** as a scaffold for preliminary SAR

TABLE 2 Described small-molecule KEAP1-NRF2 PPI inhibitors

Family	Structure	KEAP1 PDB-ID	Biological activity	References
1,2,3,4-Tetrahydroisoquinoline compounds		4L7B	IC ₅₀ (FP) = 2.3 μM K _d (SPR, competition assay) = 1.0 μM Functional cell assays: NRF2 nuclear translocation, ARE-β-lactamase reporter assay, and efflux ratio in MDCK-MDR1 cells In vivo brain exposure in mice	[73] [75]
		4L7D	IC ₅₀ (FP) = 0.75 μM	[76]
		6SP1	IC ₅₀ (TR-FRET) = 183 nM Permeability in MDCK-MDR1 cells	[77]
		6SP4	IC ₅₀ (TR-FRET) = 2.5 μM	[77]
1,4-Diaminonaphthalene-related compounds		4IQK	IC ₅₀ (FP) = 1.46 μM K _d (BLI) = 1.69 μM Metabolic stability in microsomes Functional cell assays: ARE-luciferase reporter assay, NRF2-dependent response, mitophagy activation	[78]
		-	IC ₅₀ (FP) = 28.6 nM K _d (BLI) = 9.91 nM Metabolic stability in microsomes Functional cell assays: ARE-luciferase reporter assay, NRF2-dependent response, mitophagy activation	[79]

(Continues)

TABLE 2 (Continued)

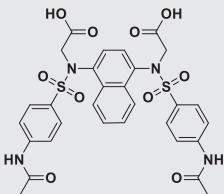
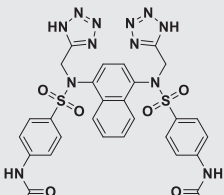
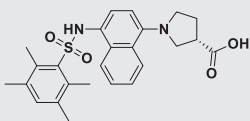
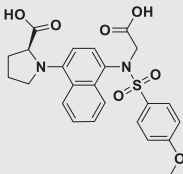
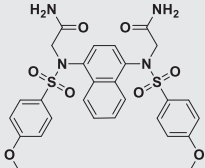
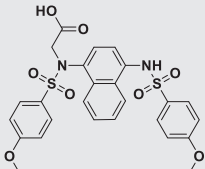
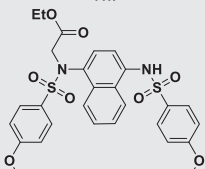
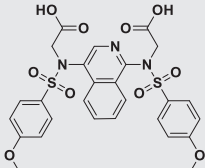
Family	Structure	KEAP1 PDB-ID	Biological activity	References
	 <p>7</p>	-	<p>IC_{50} (FP) = 14.4 nM</p> <p>K_d (ITC) = 39.8 nM</p> <p>Functional cell assays: ARE</p> <ul style="list-style-type: none"> -luciferase reporter assay, NRF2-dependent response, protection against dextran sodium sulfate in colonic cells, and LPS-induced toxicity in HK-2 human proximal tubular epithelial cells and retinal cells <p>In vivo anti-inflammatory properties in an LPS mouse model and LPS-induced mouse model of chronic renal inflammation</p> <p>In vivo mouse model of chronic ulcerative colitis</p> <p>In vivo rat model of retinal ischemia-reperfusion model</p>	[81]
	 <p>8</p>	-	<p>IC_{50} (FP) = 15.8 nM</p> <p>PAMPA assay</p> <p>Functional cell assays: ARE</p> <ul style="list-style-type: none"> -luciferase reporter assay, NRF2-dependent response 	[82]
	 <p>9</p>	5CGJ	<p>IC_{50} (FP) = 140 nM</p> <p>K_d (ITC) = 6.0 μM</p> <p>Selectivity evaluated in whole genome DNA arrays and protein panels</p> <p>Metabolic stability in microsomes</p> <p>Functional cell assays: ARE</p> <ul style="list-style-type: none"> -luciferase reporter assay, NRF2 nuclear translocation, NRF2-dependent response, anti-inflammatory properties in LPS model in macrophages <p>In vivo target engagement in liver (only observed when inhibiting oxidative hepatic metabolism)</p>	[83]

TABLE 2 (Continued)

Family	Structure	KEAP1 PDB-ID	Biological activity	References
	 10	-	IC_{50} (FP) = 43 nM K_d (ITC) = 53.7 nM; K_d (BLI) = 28.5 nM Functional cell assays: CESTA assay, ARE-luciferase reporter assay, NRF2-dependent response, cytoprotection against acetaminophen-induced hepatotoxicity In vivo mice model of acute liver failure	[84]
	 11	4XMB	IC_{50} (FP) = 63 nM K_d (SPR) = 44 nM	[85]
	 11h	6V6Z	IC_{50} (FP) = 85 nM K_d (SPR) = 400 nM	[85]
	 11i	-	IC_{50} (FP) = 61 nM K_d (SPR) = 110 nM Functional cell assays: NRF2-dependent response	[85]
	 12	-	IC_{50} (FP) = 60 nM K_d (SPR) = 102 nM Metabolic stability in microsomes Functional cell assays: NRF2-dependent response, mini-Ames test for mutagenic profile	[86]

(Continues)

TABLE 2 (Continued)

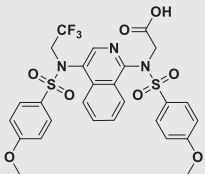
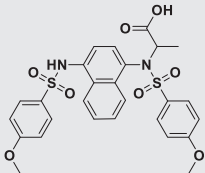
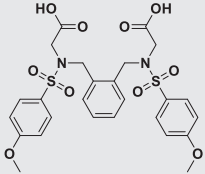
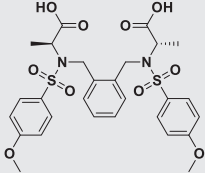
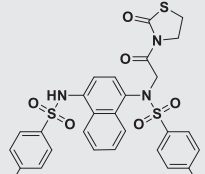
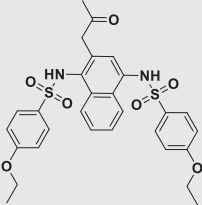
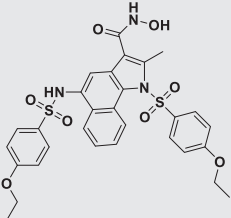
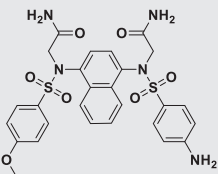
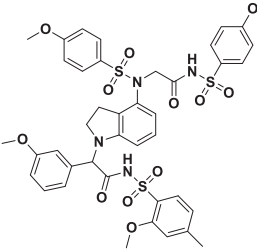
Family	Structure	KEAP1 PDB-ID	Biological activity	References
	 13	6UF0	IC_{50} (FP) = 73 nM Metabolic stability in microsomes Functional cell assays: NRF2-dependent response	[87]
	 14	-	IC_{50} (FP) = 126 nM	[88]
	 15	-	IC_{50} (FP) = 2.30 μ M Metabolic stability in microsomes	[89]
	 16	-	IC_{50} (FP) = 150 nM Metabolic stability in microsomes	[89]
	 17	-	Active following H ₂ O ₂ activation or cellular ROS stimulation PAMPA assay, psychochemical characterization Functional cell assays: ARE-luciferase reporter assay, NRF2-dependent response, antioxidant and anti-inflammatory properties in LPS model in RAW 264.7 cells In vivo pharmacokinetic parameters in rats In vivo anti-inflammatory properties in an LPS mouse model	[90]

TABLE 2 (Continued)

Family	Structure	KEAP1 PDB-ID	Biological activity	References
	 <p>18</p>	4ZY3	<p>$IC_{50} \text{ (FP)} = 6.2 \mu\text{M}$</p> <p>Selective KEAP1-p62 interaction inhibitor ($IC_{50} \text{ (FP)} = 1.5 \mu\text{M}$)</p> <p>Functional cell assays: suppression of NRF2 response and proliferation of Huh1 cancer cells</p>	[91]
	 <p>19</p>	-	<p>$IC_{50} \text{ (FP)} = 200 \text{ nM}$</p> <p>Metabolic stability in microsomes</p> <p>Functional cell assays: NRF2-dependent response, cytotoxicity in HepG2 cells</p>	[92]
	 <p>20</p>	-	<p>$IC_{50} \text{ (FP)} = 95 \text{ nM}$</p> <p>AlphaScreen assay with 20-Biotin and KEAP1 500 nM ($EC_{50} = 120 \text{ nM}$) and 1000 nM ($EC_{50} = 170 \text{ nM}$)</p> <p>In vivo $A\beta_{1-42}$ mouse model of Alzheimer's disease</p>	[93]
Indoline compounds	 <p>21</p>	-	<p>$IC_{50} \text{ (FP)} = 22.0 \text{ nM}$</p> <p>$K_d \text{ (BLI)} = 26.4 \text{ nM}$</p> <p>$K_d \text{ (ITC)} = 58.4 \text{ nM}$</p> <p>Metabolic stability in microsomes, PAMPA assay, CYP inhibition</p> <p>Functional cell assays: ARE-luciferase reporter assay, NRF2-dependent response, protection against LPS challenge in rat H9c2 cardiac cells</p> <p>In vivo pharmacokinetic parameters in rats</p> <p>In vivo target engagement in heart</p> <p>Cardioprotective effects in an in vivo mouse model of LPS-induced cardiac injury</p>	[94]

(Continues)

TABLE 2 (Continued)

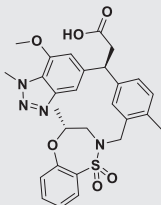
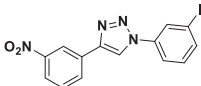
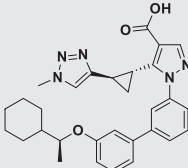
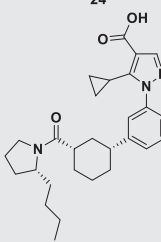
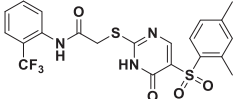
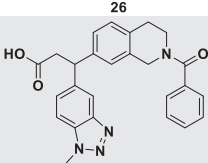
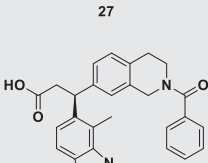
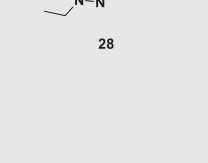
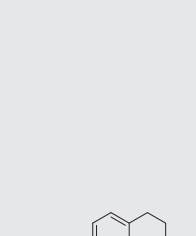
Family	Structure	KEAP1 PDB-ID	Biological activity	References
3-Phenylpropanoic acid compounds	 22	5FNU	$IC_{50} \text{ (FP)} = 95\% \text{ @ } 15 \text{ nM}$ $K_d \text{ (ITC)} = 1.3 \text{ nM}$ Selectivity against GSK's Enhanced Cross-screen Panel (eXP) Functional cell assays: NRF2-dependent response, NRF2 nuclear translocation, prevented GSH depletion, phagocytic capacity in COPD patient-derived cells In vivo target engagement in lung In vivo assessment in COPD-related models	[95, 96]
1,4-Diphenyl-1,2,3-triazole compounds	 23		$\% \text{ Inhibition (FP)}: 67.2\% (100 \mu\text{M});$ $IC_{50} \text{ (FP)} = 7.1 \mu\text{M}$ Reversibility KEAP1-binding assay Functional cell assays: NQO1 induction assay, NRF2 nuclear translocation, NRF2-dependent response, NRF2-KEAP1 interaction disruption in live cells (FRET), mitophagy activation	[97]
1-Phenylpyrazole core	 24		$IC_{50} \text{ (FP)} = 10\text{--}100 \text{ nM}$ $IC_{50} \text{ (TR-FRET)} < 10 \text{ nM}$ Functional cell assays: BEAS-2B NQO1 activity	WO20170-60854
	 25		$IC_{50} \text{ (FP)} = 10\text{--}100 \text{ nM}$ $IC_{50} \text{ (TR-FRET)} = 10\text{--}100 \text{ nM}$ Functional cell assays: BEAS-2B NQO1 activity	WO20170-60855

TABLE 2 (Continued)

Family	Structure	KEAP1 PDB-ID	Biological activity	References
Benzenesulfonyl- pyrimidone compounds		4IN4	IC ₅₀ (FP) = 118 μM	[78]
3-(1,2,3,4- tetrahydroisoquinolin- 1-yl)propanoic acid compounds		-	K _d (SPR) = 56 nM Functional cell assays: NRF2 nuclear translocation	[98]
		6TYP	K _d (SPR) = 2.7 nM Functional cell assays: NRF2 nuclear translocation Metabolic stability in microsomes, CYP, hERG inhibition Functional cell assays: NRF2 nuclear translocation, NRF2-dependent response, and cytoprotection in human spinal cord astrocytes, efflux ratio in MDCK-MDR1 cells In vivo brain exposure in mice and pharmacokinetic parameters in rats In vivo target engagement in kidney	[98]
		-	K _d (SPR) = 0.7 nM	[98]
Ureas/ hydrazinecarbohydra- zide cores		-	KEAP1 binding (SPR)	[99]

(Continues)

TABLE 2 (Continued)

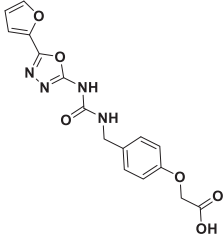
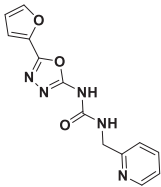
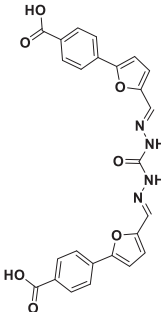
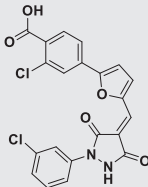
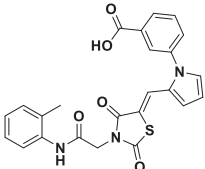
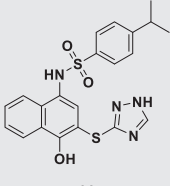
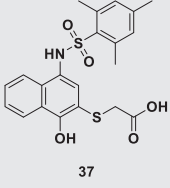
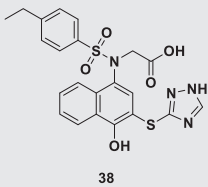
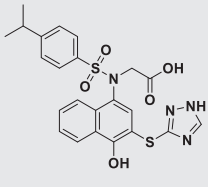
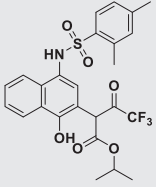
Family	Structure	KEAP1 PDB-ID	Biological activity	References
	 <p>31</p>	3VNH 3VNG	KEAP1 binding (SPR) NRF2-KEAP1 PPI inhibition (AlphaScreen)	[99]
	 <p>32</p>	-	KEAP1 binding (SPR) Functional cell assays: ARE -luciferase reporter assay, cytoprotection against H2O2 toxicity in Huh-7 cells In vivo rat model of diet-induced nonalcoholic steatohepatitis	[100]
	 <p>33</p>	-	IC ₅₀ (FP) = 9.80 mM Functional cell assays: ARE -luciferase reporter assay	[101]
Pyrazolidine-3,5-dione compounds	 <p>34</p>	-	IC ₅₀ (FP) = 15.2 μM DSF assay	[102]
Thiazolidine-2,4-dione compounds	 <p>35</p>	-	IC ₅₀ (FP) = 10.4 μM DSF assay	[102]

TABLE 2 (Continued)

Family	Structure	KEAP1 PDB-ID	Biological activity	References
4-Aminonaphthalen-1-ol compounds	 36	-	$IC_{50} \text{ (FP)} = 2.9 \mu\text{M}$ DSF assay functional cell assays: NRF2 nuclear translocation, NRF2-dependent response	[102]
	 37	-	$IC_{50} \text{ (FP)} = 4.2 \mu\text{M}$	[102]
	 38	-	$IC_{50} \text{ (FP)} = 1.14 \mu\text{M}$ $K_d \text{ (SPR)} = 453 \text{ nM}$ DSF assay Functional cell assays: NRF2 nuclear translocation, NRF2-dependent response, protection against LPS challenge in rat H9c2 cardiac cells Cardioprotective effects in an in vivo mouse model of LPS- induced acute death	[103]
	 39	-	$IC_{50} \text{ (FP)} = 8.52 \mu\text{M}$ $K_d \text{ (SPR)} = 5170 \text{ nM}$ DSF assay Functional cell assays: NRF2 nuclear translocation, NRF2-dependent response, protection against LPS challenge in rat H9c2 cardiac cells Cardioprotective effects in an in vivo mouse model of LPS- induced acute death	[103]
	 40	-	$IC_{50} \text{ (FP)} = 3 \mu\text{M}$ $K_d \text{ (SPR)} = 1.7 \mu\text{M}$ Functional cell assays: NRF2 nuclear translocation, ARE- β -lactamase reporter assay	WO20130- 67036

(Continues)

TABLE 2 (Continued)

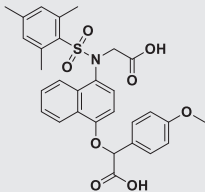
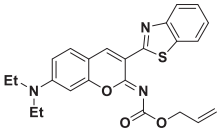
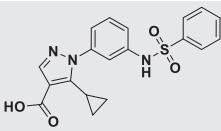
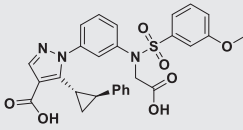
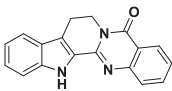
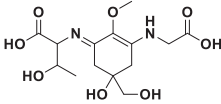
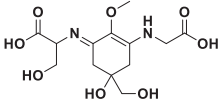
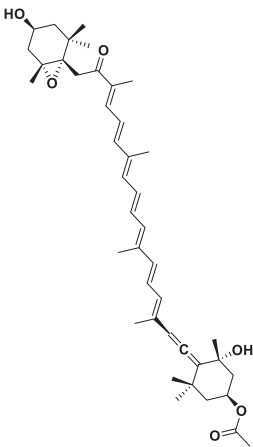
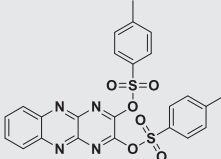
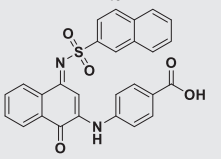
Family	Structure	KEAP1 PDB-ID	Biological activity	References
	 41	-	$IC_{50} \text{ (FP)} = 75 \text{ nM}$ $K_d \text{ (BL)} = 36.5 \text{ nM}$ $K_d \text{ (ITC)} = 24.0 \text{ nM}$ Metabolic stability in microsomes, CYP inhibition Functional cell assays: ARE -luciferase reporter assay, NRF2 nuclear translocation, NRF2-dependent response, antioxidant and anti-inflammatory properties in LPS model in RAW 264.7 cells In vivo pharmacokinetic parameters in rats In vivo anti-inflammatory properties in an LPS mouse model	WO20171-24835 [104]
Iminocoumarin-benzothiazole compounds	 42	-	$IC_{50} \text{ (FP)} = 5.1 \text{ mM}$ $K_d \text{ (SPR)} = 48.1 \text{ mM}$ Functional cell assays: NRF2 nuclear translocation, antioxidant and anti-inflammatory properties in LPS model in H9c2 cells In vivo mouse model of LPS-induced septic cardiomyopathy In vivo mouse model of hyperoxic acute lung injury	[105, 106]
N-(3-(1H-pyrazol-1-yl)phenyl) benzenesulfonamide compounds	 43	6ZEY	43: $IC_{50} \text{ (FP)} = 15.6 \text{ }\mu\text{M}$ PAMPA assay Microsomal stability Blood plasma stability	[107]
	 44	6ZF8	44: $IC_{50} \text{ (FP)} = 0.040 \text{ }\mu\text{M}$ PAMPA assay Microsomal stability Blood plasma stability	[107]

TABLE 2 (Continued)

Family	Structure	KEAP1 PDB-ID	Biological activity	References
Natural products	 <p>45</p>	-	K_d (SPR) = 19.6 μ M Functional cell assays: NRF2 nuclear translocation, protection against H ₂ O ₂ in HCT116 cells Anti-inflammatory and protection in an in vivo mouse model of DSS-induced colitis	[108]
	 <p>46</p>	-	IC_{50} (FP) ~ 100 μ M DSF assay	[109]
	 <p>47</p>	-	IC_{50} (FP) ~ 100 μ M DSF assay	[109]
	 <p>48</p>	-	K_d (BLI) = 51.6 μ M Functional cell assays: ARE-luciferase reporter assay, NRF2 nuclear translocation, NRF2-dependent response, antioxidant and anti-inflammatory properties in 6-OHDA model in PC12 cells Protection and antioxidant effect in an in vivo 6-OHDA-injured zebrafish model	[110]
Other compounds	 <p>49</p>	-	IC_{50} (FP) = 0.258 μ M	[111]
	 <p>50</p>	-	IC_{50} (FP) = 2.7 μ M	[111]

(Continues)

TABLE 2 (Continued)

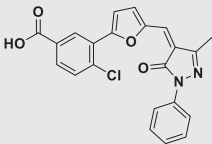
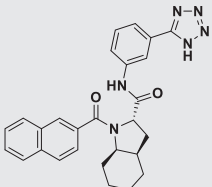
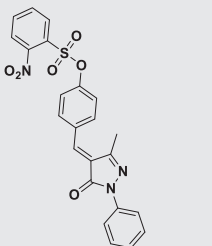
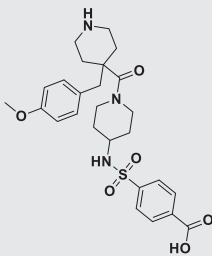
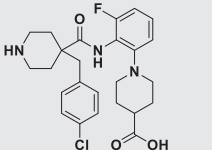
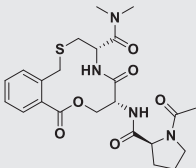
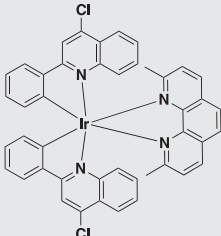
Family	Structure	KEAP1 PDB-ID	Biological activity	References
	 51	-	IC ₅₀ (FP) = 38.2 μM	[111]
	 52	-	IC ₅₀ (FP) = 14.2 μM	[111]
	 53	-	Pull-down assay for KEAP1-NRF2 interaction PAMPA assay, oral bioavailability Functional cell assays: NRF2 nuclear translocation, NRF2-dependent response, anti-inflammatory effect in LPS-stimulated BV-2 cells, NRF2-dependent anti-inflammatory effect in BV-2 cells In vivo MPTP-induced mouse model of PD	[112]
	 54	-	85.5% inhibition at 100 μM (TR-FRET)	[113]
	 55	-	74.3% inhibition at 100 μM (TR-FRET)	[113]

TABLE 2 (Continued)

Family	Structure	KEAP1 PDB-ID	Biological activity	References
	 56	6Z6A	K_d (ITC) = 3.7 μ M K_d (SPR) = 4.1 μ M Aqueous solubility determination, metabolic stability in microsomes, Caco-2 cells permeability assay Functional cell assays: NRF2 nuclear translocation	[114]
	 57	-	IC_{50} (FP assay) = 1.09 μ M K_d (ITC) = 0.71 μ M, ΔG = -8.39 kcal/mol, ΔH = -6.75 kcal/mol, $-T\Delta S$ = -1.64 kcal/mol. Functional cell assays: NRF2 nuclear translocation, NRF2-dependent response, protection against acetaminophen challenge in LO2 cells In vivo pharmacokinetic parameters in mice In vivo toxicity evaluation. Protection against acetaminophen hepatotoxicity in an in vivo mice model	[115]

Abbreviations: ARE, antioxidant response element; COPD, chronic obstructive pulmonary disease; CYP, cytochrome P450; DSF, differential scanning fluorimetry; DSS, dextran sulfate sodium; FP, fluorescence polarization; ITC, isothermal titration calorimetry; KEAP1, Kelch-like ECH-associated protein 1; LPS, lipopolysaccharide; LPS, lipopolysaccharide; MPTP, 1-methyl-4-phenyl-1,2,3,6-tetrahydropyridine; NQO1, NAD(P)H:quinone oxidoreductase 1; NRF2, nuclear factor erythroid 2-related factor 2; PAMPA, parallel artificial membrane permeability assay; PD, Parkinson's disease; ROS, reactive oxygen species; SPR, surface plasmon resonance; TR-FRET, time-resolved fluorescence resonance energy transfer.

studies and a posterior peptide SAR study with a small library of 70 analogs of 9mer LDEETGEFL with substitutions at Glu82 position. The conclusions of this study determined that the inclusion of glycol or hydroxyl substituents at THIQ system position 5 led to increased activity (compounds **3a–g** for SAR, Supporting Information: Table S2). Compound **3** (Table 2) showed an IC_{50} value of 183 nM, compared to IC_{50} = 792 nM of compound **1**. Then, cyclobutyl carboxamide moiety was introduced resulting in a retained activity compared to cyclobutyl acidic analogs as shown for compound **4** (Table 2) (IC_{50} = 2.5 μ M), although it was less potent than compound **3** (compounds **4a–e** for SAR, Supporting Information: Table S2). X-ray crystallographic studies revealed new interactions for compounds **3** (PDB-ID **6SP1**) and **4** (PDB-ID **6SP4**). Moreover, the carboxamide analog showed a five-fold permeability improvement in MDCK cells compared to acidic derivative **3**, although it was less active for PPI inhibition.⁹⁰

3.2.2 | 1,4-Diaminonaphthalene-related compounds

Following the discovery of THIQ compounds as the first small molecules targeting KEAP1-NRF2 interaction, Marcotte et al.¹¹⁶ from Biogen identified compound **5** as a moderate PPI inhibitor. An HTS program based on a homogeneous confocal fluorescence anisotropy assay (two-dimensional fluorescence intensity distribution analysis (2D-FIDA) as KEAP1-NRF2 competition FP assay) was performed against about 270,000 compounds from Evotec Lead Discovery library plus 1911 compounds identified from a virtual screening as KEAP1 Kelch domain binders. Hit compound **5** (**Cpd16**, Table 2) showed an IC_{50} value of 2.7 μ M (2D-FIDA assay), increased NRF2-dependent luciferase activity in a DLD1 cell-based reporter assay and NQO1 protein levels demonstrating its capacity to activate the phase II antioxidant response. **Cpd16**-KEAP1 Kelch domain cocrystal structure (PDB-ID **4IQK**) confirmed its binding at the central cavity, highlighting an important cation- π stacking interaction between side chain of Arg415 and the electron-rich naphthalene core. Mass spectrometry with full-length KEAP1 and nuclear magnetic resonance (NMR) experiments performed with Kelch domain expressed with N¹⁵-labeled arginines and nitrogens on Arg415, Arg483, and Arg380 confirmed its binding at the central cavity and the absence of covalent cysteine reactivity for **5**.¹¹⁶

Considering **5** as a scaffold for structure-based design and regarding energetic contributions for the KEAP1-NRF2 interaction analyzed by molecular dynamics and MM-GBSA calculations, Jiang et al.⁹¹ developed compound **6** (**CPUY192002**, Table 2). **5** sulfonamide groups introduce *N*-acetic acid moieties to generate **6** with highly improved PPI inhibitory potency (IC_{50} = 28.6 nM measured by FP assay, and K_d = 9.91 nM measured by biolayer interferometry assay for interaction with KEAP1), compared to **5** (IC_{50} = 1.46 μ M (FP assay) and K_d = 1690 nM (BLI)). Regarding its in vitro cellular evaluation, it induced a strong NRF2-dependent response in the HepG2-ARE-C8 cells (ARE-luciferase reporter assay), and increased the expression of NRF2-related genes (GCLM, HO-1, and NQO1) in HCT116 cells. Nevertheless, **6** has a low pK_a value (pK_a = 4.72) that may restrict passive diffusion limiting membrane permeability and thus cellular activity.⁹¹ Additionally, compound **6** was recently evaluated as a novel strategy for chronic obstructive pulmonary disease (COPD) therapy. After treatment with **6**, oxygen consumption and extracellular acidification rate (OCR/ECAR), which is decreased in macrophages from COPD patients, was augmented. In these human COPD alveolar macrophages (AM), **6** led to a dose-dependent increase in NRF2 nuclear translocation and NRF2-dependent protein levels (HO-1, NQO1, and GST). Importantly, **6** also ameliorated impaired phagocytic ability of mice AM on *Haemophilus influenzae* and *Streptococcus pneumoniae* following cigarette smoke condensate (CSC) exposure in a dose-dependent manner. This effect was also reproduced with COPD AM and, interestingly, this beneficial effect was lost in Nfe2l2 knockout mice cells. Finally, **6** showed a good profile in the COPD mice model generated upon CSC exposure. It induced NRF2 nuclear accumulation and markedly resumed phagocytosis in mice AM, enhanced the OCR/ECAR ratio, and reduced pro-inflammatory factors production in lung tissue (interferon production regulator (IFN γ), IL-5, IL-6, and TNF- α).¹¹⁷

In this sense, several structural modifications based on these previous scaffolds have been evaluated, trying to optimize their drug-like properties. From a subset of compound **6** derivatives bearing different substituents at benzenesulfonyl rings or with a modification of naphthalene to phenyl ring, *p*-acetamido compound **7** (named **CPUY192018**, Table 2) resulted the most promising. Analysis of this set of compounds concluded that the naphthalene core is a key pharmacophore for KEAP1-NRF2 PPI inhibition (compounds **7a–e** for naphthalene to phenyl ring SAR, **7f–s** for SAR at benzenesulfonyl ring position, Supporting Information: Table S2).¹¹⁸ Compared to **6**, **CPUY192018** or **7** exhibited slightly better PPI inhibition activity (IC_{50} = 14.4 nM by FP assay), higher solubility (5.0 mg/ml compared to 0.388 mg/ml of **6**), and higher NRF2 induction capacity in the ARE-luciferase reporter assay performed in HepG2-ARE-C8 cells (twofold increased potency compared to **6**). Derivative **7** increased NRF2-dependent protein levels in HCT116 cells (NQO1, HO-1, and γ -GCS) and was selected for in vivo evaluation. It showed interesting anti-inflammatory properties in an LPS mouse model. Mice were pretreated with **7** for 3 days and then challenged with LPS 24 h after the last dose of the compound. Samples were collected 5 h post-LPS

challenge, showing that **7** was able to significantly and dose-dependently reduce pro-inflammatory cytokines levels: TNF- α , IFN- γ , IL-6, IL-12, and IL-17.¹¹⁸

Encouraging results demonstrated by compound **7** prompted its optimization by bioisosteric substitutions at the *N*-acetic acid moieties.⁹² Pharmacological evaluation of compound **7** analogs, led to the selection of hit compound **8** bearing a di-tetrazole substitution which maintained potent PPI inhibitory activity (IC_{50} = 15.8 nM by FP assay) with additional improvements in drug-like properties (compounds **8a–c** for SAR, Supporting Information: Table S2). Compound **8** showed higher pK_a and $\log D_{pH=7.4}$ values than **7**, properties that could promote passive cell membrane permeability, and retained solubility. Parallel artificial membrane permeability assay (PAMPA) confirmed this improvement, showing more than a 100-fold increase in permeability coefficients of **8**, which also demonstrated higher NRF2 induction capacity in the HepG2-ARE-C8 cell line and increased NRF2-dependent gene expression (HO-1, NQO1, and GCLm) and protein levels in HCT116 cells (HO-1, NQO1, and γ -GCS).⁹²

A screening effort followed by a medicinal chemistry program by Winkel et al. from Sanofi¹¹⁹ resulted in a new hit, compound **9** (RA839, Table 2), one of the first asymmetric 1,4-diaminonaphthalene compounds. Compound **9** showed an IC_{50} value of 140 nM (FP assay) and a KEAP1 Kelch domain binding K_d value of 6 μ M measured by ITC. Cocrystal structure with this domain (PDB-ID 5CGJ revealed similar binding mode to compound **5**, maintaining key Arg415 interaction, but in this case exhibiting important direct interaction between carboxylic moiety of **9** and Arg483 side chain. Compound **9** cellular activity was confirmed in ARE-luciferase reporter assay in HepG2 cells, and induced NRF2 nuclear translocation in PathHunter U2OS KEAP1-NRF2 functional assay. Remarkably, whole genome DNA arrays showed that compound **9** was able to regulate 105 probe sets in bone marrow-derived macrophages. Target selectivity was further demonstrated as no interaction with a panel of 93 proteins (unrelated enzymes, receptors, and channels). Additionally, **9** exhibited anti-inflammatory properties being able to suppress nitric oxide (NO) production and inducible nitric oxide synthase 2 (iNOS2) expression in LPS-treated macrophages. More importantly, compound **9** upregulated NRF2-dependent genes in vivo in mice (increased hepatic mRNA levels of NQO1 and GCLm). However, NRF2 target genes upregulation in mice was only observed when using a cytochrome P450 inhibitor which reduced oxidative hepatic metabolism, as **9** suffers a high metabolic turnover, revealing the necessity to improve its drug-like properties.¹¹⁹

Recent work by Lu et al.¹²⁰ reported a novel family of **6** derivatives in which they incorporate α -amino acid substituents into the naphthalene-sulfonamide scaffold leading to novel nonasymmetric compounds. SAR studies included aliphatic, polar, and ring-containing amino acid substituents from which Pro and Phe derivatives showed the best properties in this new attempt to improve drug-like properties of former compound **6** (compounds **10a–aa** for SAR, Supporting Information: Table S2). Remarkably, Pro derivative **10** (Table 2) was the most potent KEAP1-NRF2 PPI inhibitor showing an IC_{50} value of 43 nM in the competitive FP assay and a KEAP1 binding K_d of 53.7 nM and 28.5 nM measured by ITC and BLI, respectively. Additionally, **10** exhibited target engagement in cells measured by cellular thermal shift assay (CESTA), it increased luciferase activity in the ARE-luciferase reporter assay performed in HepG2-ARE-C8 cells, and showed increased NRF2-dependent gene expression and protein levels (NRF2, HO-1, NQO1, and GCLm) in hepatic L02 cells. Interestingly, **10** also prevented acetaminophen-induced hepatotoxicity in vitro in L02 cells (cell viability recovery, reduced apoptosis rate, decrease in the production of pro-inflammatory factors such as IL-1 β , IL-6, and TNF- α , and upregulation of oxidative-related GSH/GSSG ratio, among other results). Compound **10** also showed promising result in vivo in a mice model of acute liver failure (ALF), reducing liver damage measured by different markers, and decreasing pro-inflammatory cytokines serum levels such as IL-1 β , IL-6, and TNF- α , among other results).¹²⁰ Interestingly, previously introduced compound **9** contains a pyrrolidine-3-carboxylic acid similar to Pro revealing this pyrrolidine ring as promising moiety for KEAP1-NRF2 inhibitors.

In parallel to previous research, Jain et al.¹²¹ and subsequent works by this group reported several families of **5** and **6** derivatives with extensive SAR.^{93,94,122} First, they evaluated benzenesulfonyl substituents, *N*-acetic acid replacements, and naphthalene substitution patterns and reported that acetic acid moieties are not essential to

maintain PPI inhibitory activity, a key conclusion for the development of novel compounds with improved drug-like properties (compounds **11a–j** for SAR, Supporting Information: Table S2). A highlighted example is compound **11** (Table 2), an *N*-diacetamide analogue of **5**, which maintained activity in nanomolar range ($IC_{50} = 63$ nM by FP assay; KEAP1 binding $K_d = 44$ nM by SPR). Cocrystal structure with KEAP1 Kelch domain PDB-ID **4XMB** confirmed its binding mode. They also highlighted singly substituted *N*-acetic acid compound **11h** ($IC_{50} = 61$ nM by FP assay; KEAP1 binding $K_d = 110$ nM by SPR) and singly substituted *N*-ethyl acetate **11i** ($IC_{50} = 85$ nM by FP assay; KEAP1 binding $K_d = 400$ nM by SPR). In vitro cellular evaluation of **11i** showed increased protein levels of HO-1 and NRF2 in a mouse lung alveolar epithelial cell line (MLE12).¹²¹ Thereafter, 10 different naphthalene replacements were evaluated aiming to improve drug-like properties and regarding potential metabolite reactivity derived from naphthalene core (compounds **12a–e** for SAR, Supporting Information: Table S2).¹²² Among them, 1,4-isoquinoline scaffold exemplified by compound **12** (Table 2) showed a better mutagenic profile as proven by a mini-Ames assay, without losing potency ($IC_{50} = 60$ nM by FP assay; KEAP1 binding $K_d = 102$ nM by SPR), increased metabolic stability (mouse and human liver microsomes), and higher solubility compared to **6**. Compound **12** also maintained cellular activity in nontransformed immortalized human keratinocytes (HaCaT cells) being able to induce NRF2-dependent gene expression and to increase phase II response protein levels (NQO1, GCLm, cytosolic and nuclear NRF2). However, its low $\log D_{pH=7.4}$ (−1.5) and its negative charge at physiological pH could limit its membrane permeability, similarly to previous carboxylic acid-bearing derivatives. Thus, Lazzara et al.⁹³ reported a new series of derivatives with different benzenesulfonyl substituents and *N*-acetic acid replacements (compounds **13a–n** for SAR, Supporting Information: Table S2). Hit compound **13** (PRL-295, Table 2), obtained by replacing carboxymethyl group at 4-position of **12** by a trifluoroethyl group, maintained KEAP1-NRF2 PPI inhibitory potency ($IC_{50} = 73$ nM by FP assay), enhanced metabolic stability (human liver microsomes), and showed a better profile in membrane permeability (increased $\log D_{pH=7.4}$ to 0.5). **13**-KEAP1 Kelch domain cocrystal (PDB-ID **6UFO**) revealed important interactions between its carboxylate moiety and close arginine residues (Arg380 and Arg415).⁹³ In a recent work by this group, Lazzara et al.⁹⁴ reported new SAR evaluation of single sulfonamide and sulfone derivatives, however, they observed an affinity drop compared to **13** parental compounds (compounds **14a–e** for SAR, Supporting Information: Table S2). Thus, they explored novel α -amino substituents maintaining symmetric bis-sulfonamide or sulfonamide-sulfone scaffold (compounds **14f–j** for SAR, Supporting Information: Table S2). These modifications were exemplified by compound **14** (Table 2) with nanomolar PPI inhibitory activity.⁹⁴

Many small derivatives exhibited potent KEAP1-NRF2 PPI inhibitory activity, however, most of them revealed issues related to their cellular membrane permeability, stability, or their inability to cross the BBB. In that sense, Abed et al.⁹⁶ (Rutgers University), recently developed several new families of compounds based on substitutions of the naphthalene core and other structural changes from former compound **6**. Initial efforts led to the 1,2-disubstituted xylene analog **15** ($IC_{50} = 2.30$ μ M by FP assay, Table 2) and its further optimization (compounds **16a–f** for SAR, Supporting Information: Table S2). Among them, compound **16** showed the most potent PPI inhibitory activity ($IC_{50} = 150$ nM measured by FP assay). Importantly, compounds **15** and **16** exhibited improved metabolic stability (human liver microsomes) compared to parental compound **6**. After 90 min of incubation **15** and **16** maintained stable (97.7% and 98.2% remaining, respectively) in contrast to **6** (56.9% remaining).⁹⁶

Pursuing drug-like properties optimization, Jiang group described recently a highly interesting development on KEAP1-NRF2 PPI inhibitors with improved physicochemical properties and cell membrane permeability.¹²³ Albeit most PPI inhibitors described previously showed nanomolar potency in in vitro isolated PPI inhibition evaluation, micromolar levels are needed to obtain biological effect once in cellular or in vivo evaluations.⁹⁵ Ionizable carboxylic groups present in most of these compounds could explain their low permeability. To overcome these limitations, these authors developed ROS-responsive prodrugs by adding a thiazolidinone protecting group to the carboxylic acid moieties of its previous compound **6** (bearing two carboxylic acid groups) and **11h** (bearing one carboxylic acid group and just a moderate decrease in activity compared to **6**, also reported previously by Jain et al.¹²¹). In presence of H_2O_2 , prodrug containing two thiazolidinone moieties was hydrolyzed to generate the compound with only one free carboxylic acid, thus they selected compound **17** bearing one thiazolidinone group for further studies.

Compound **17** was stable and inactive under normal physiological conditions, becoming active in presence of H_2O_2 or inflammation-derived ROS. Compound **17** exhibited better physicochemical properties and cell membrane permeability (PAMPA assay) compared to **11 h**. Following LPS activation for intracellular ROS production, **17** showed improved activity in the ARE-luciferase reporter assay in HepG2-ARE-C8 cells ($\text{EC}_{50} = 0.32 \mu\text{M}$ compared to $\text{EC}_{50} = 13.14 \mu\text{M}$ for **11 h**). Under these conditions, it also led to higher NRF2-dependent gene expression and protein levels (HO-1, NQO1, and GCLm) in mouse RAW 264.7 cells. Interestingly, **17** improved antioxidant capacity (superoxide dismutase [SOD] and glutathione peroxidase [GSHPx] activities), and reduced pro-inflammatory factors induced by LPS (IL-1 β , IL-6, TNF- α , and NO). Moreover, **17** displayed good pharmacokinetic profile in oral administration and enhanced anti-inflammatory efficiency in vivo against the LPS challenge (decreased IL-1 β , IL-6, TNF- α , and IFN γ serum levels). By using this strategy, not only pharmacokinetic properties were improved, but also it is possible to have a compound being active only in pathological cells while not affecting normal cells, and thus avoiding undesirable effects from NRF2 induction.¹²³

Saito et al.⁹⁷ reported compound **18** (K67, Table 2), a structural analogue of **5**, bearing a 2-oxopropyl moiety at 2-position of the naphthalene ring. They performed an FP-based HTS of 155,000 compounds of the Drug Discovery Initiative at the University of Tokyo using recombinant KEAP1 Kelch domain as protein target and the 6-FAM (6-carboxyfluorescein)-labeled S349-phosphorylated peptide of p62 as fluorescent probe. With this strategy, they intended to achieve selective inhibitors of KEAP1-p62 PPI to inhibit the NRF2 pathway in the search of potential antitumor drugs. As previously described, NRF2 activation is positively regulated by the PPI between KEAP1 and p62. p62 competes with NRF2 to bind KEAP1 disrupting DLG low-affinity motif, without altering the ETGE high-affinity interaction (five-fold weaker interaction compared to the DLG low-affinity motif). Thus, KEAP1-p62 PPI inhibitors are able to inactivate the NRF2-ARE pathway. As p62 binds to KEAP1 in the same pocket as NRF2, it is expected that compounds targeting this interaction show KEAP1-NRF2 PPI activity. **18**-KEAP1 Kelch domain X-ray cocrystal structure (PDB-ID 4ZY3) demonstrated similar binding mode to analogue compound **5** at the bottom of the β -propeller structure close to basic amino-acid residues and exhibiting key cation- π interaction with Arg415. In vitro pull-down assays demonstrated that both **18** and **5** were capable of inhibiting the interaction between KEAP1 and phosphorylated p62, but only **5** disturbed KEAP1 and NRF2 interaction, thus, **18** was considered specific KEAP1-p62 PPI inhibitor. Moreover, **18** suppressed NRF2 target genes expression and cellular proliferation of Huh1 cancer cells.⁹⁷ Subsequent SAR study on **18** scaffold by Yasuda et al.¹²⁴ proved KEAP1-NRF2 interaction inhibition of **18** by FP assay ($\text{IC}_{50} = 6.2 \mu\text{M}$), although it was more potent and selective for the KEAP1-p62 PPI inhibition ($\text{IC}_{50} = 1.5 \mu\text{M}$). Further evaluation of compound **18** analogs reported novel KEAP1-NRF2 PPI at the low micromolar range with various side chains at naphthalene ring 2-position. Although they all showed KEAP1-p62 inhibition and none of them was more selective for NRF2 (compounds **18a-h** for SAR, Supporting Information: Table S2).¹²⁴ Extensive SAR study at four position of the two benzenesulfonyl groups of **18** yielded novel derivatives without improving potency for neither p62 nor NRF2 interaction, nonetheless, some of them showed increased properties to overcome chemoresistance in Huh1 cancer cells (compounds **18i-n** for SAR, Supporting Information: Table S2).¹²⁵

Previously reported FP-based HTS of Drug Discovery Initiative library for KEAP1-p62 interaction⁹⁷ gave also compound **19**, a **5** and **18** analogue, containing a unique benzo[g]indole skeleton and an indole-3-hydroxamic acid moiety (Table 2).¹²⁶ This compound showed potent KEAP1-NRF2 PPI inhibition ($\text{IC}_{50} = 200 \text{ nM}$ by FP assay), exhibited cellular target engagement increasing NQO1 expression in MEF cells, and eight times higher metabolic stability than **5** (human liver microsomes) with low hepato-cytotoxicity in HepG2 cells. Several hydrazide derivatives of **19** were reported as KEAP1-NRF2 PPI inhibitors with slightly higher potency and maintained metabolic stability indicating the interest of the benzo[g]indole core for further developments (compounds **19a-e** for SAR, Supporting Information: Table S2).¹²⁶

The importance of the discovery of this class of compounds is reflected in some novel applications that have been developed. In particular, compound **6** has been used to integrate several reporter groups to obtain biological probes. Lu et al.¹²⁷ developed probe **P1** with a biotin tag and probe **P2** with a FITC both linked to **6** scaffold at the

benzenesulfonyl ring using a linker, without missing KEAP1 binding affinity (Supporting Information: Table S2). On the one hand, **P1** has been effectively used in a pull-down assay to capture cellular KEAP1 by bounding streptavidin coupled magnetic beads after incubation with normal human colon mucosal epithelial cell line (NCM460) colonic cell lysates. On the other hand, **P2** could be used to target cellular KEAP1 in fluorescence microscopy experiments as proven also with NCM460 colonic cells.¹²⁷

After this intensive evaluation of KEAP1-NRF2 PPI inhibitors, **7** (named as **CPUY192018**), demonstrated the most interesting properties. Its effectiveness has been evaluated in different disease models both in vitro and in vivo,^{13,98,99} revealing a multitarget profile and the high interest of noncovalent NRF2 activators. Compound **7** provided protection against dextran sodium sulfate in both NCM460 colonic cells and in an in vivo mouse model of chronic ulcerative colitis, attenuating inflammation and oxidative stress in colon.⁹⁸ Similarly, it was found to be protective against LPS-induced toxicity in human kidney 2 (HK-2) proximal tubular epithelial cells and also in an LPS-induced mice model of chronic renal inflammation. Renal protection was associated to the activation of the NRF2-dependant antioxidant response and the inhibition of the NF- κ B mediated inflammatory response.¹³ Furthermore, a recent study with **7** demonstrated its therapeutic potential for retinal ischemia. It activated the NRF2 pathway to afford protection in human retinal endothelial cells (HREC) against oxidative stress and LPS-induced inflammatory injury. Importantly, both topical and systemic administration of **7** rescued visual function in the retinal ischemia-reperfusion model performed in rats with clear NRF2 gene upregulation in the retina.⁹⁹ Another important finding was made by Sun et al.¹²⁸ who reported one of the first evaluations of a KEAP1-NRF2 PPI inhibitor in an AD mouse model. They developed a new asymmetric 1,4-diaminonaphthalene derivative **20** (**NXPZ-2**, Table 2). Compound **20** showed a potent KEAP1-NRF2 inhibition (IC_{50} = 95 nM by FP assay) and exhibited positive results in an AD mouse model induced by intracerebroventricular amyloid beta 1-42 ($A\beta_{1-42}$) injection. Briefly, **20** restored cognitive decline induced by $A\beta_{1-42}$, showed neuroprotective properties and target engagement leading to NRF2 activation in brain structures as cortex and hippocampus. Importantly, its therapeutic effect was completely lost in an *Nfe2l2* knockout mice model.¹²⁸

3.2.3 | Indoline compounds

In a recent work by Jiang's group, Zhou et al.¹⁰⁰ reported a new family of compounds bearing a novel indoline scaffold substituting the naphthalene structure. Additionally, replacing the acetic acid groups with acylsulfonamide moieties retained a potent KEAP1-NRF2 PPI inhibitory activity. Overall, these authors performed an exhaustive SAR over a family of 93 derivatives, systematically exploring different substitution patterns. Results led to the selection of compound **21** (Table 2; compounds **21a-az** for previous SAR, Supporting Information: Table S2) with good human microsomal stability, improved gastrointestinal PAMPA permeability in comparison to **6**, low inhibition of cytochrome P450 (CYP) isozymes, and favorable in vivo pharmacokinetic parameters. Compound **21** was shown to activate NRF2-dependent response, being more potent than sulforaphane in the ARE-luciferase reporter assay performed in HepG2-ARE-C8 cells. NRF2 induction capacity was also demonstrated by the increase of NRF2-dependent gene expression and protein levels (NRF2, HO-1, NQO1, and GCLm) in rat H9c2 cardiac cells. Interestingly, **21** exhibited good anti-inflammatory properties against LPS-induced injury in both H9c2 cells and an in vivo mouse model of cardiac injury. In this line, compound **21** reduced levels of pro-inflammatory cytokines in serum (IL-1 β , IL-6, and TNF- α) and ameliorated damage and inflammation of heart tissue, reducing ROS and upregulating the GSH/GSSG ratio. Importantly, target engagement was measured in the heart in terms of increased protein levels of NRF2, HO-1, NQO1, and GCLm.¹⁰⁰

3.2.4 | 3-Phenylpropanoic acid compounds

Davies et al.¹⁰¹ (Astex Pharmaceuticals and GlaxoSmithKline Pharmaceuticals) reported the development of the novel lead compound **22** (KI-696, Table 2) discovered following a fragment-based drug discovery approach. They performed an X-ray crystallographic screening of approximately 330 fragments toward mouse KEAP1 Kelch domain and they were able to identify three hot spots within the KEAP1-NRF2 interface. These promising fragments established key interactions with Arg483, Tyr525, and Ser602, respectively, and determined the so-called “acidic,” “planar acceptor,” and “sulfonamide” pockets. Based on these findings, a phenylacetic acid fragment occupying acid pocket was used as an anchor fragment for compound growing and rational drug design. SAR was performed first in the planar acceptor and then sulfonamide pockets for optimizing compound potency, using FP and ITC assays as evaluation methods. After trying different aromatic substituents in the planar acceptor site, they reported improved compound **22c** (Supporting Information: Table S2) bearing a benzotriazole moiety directly attached to the benzylic carbon of the phenylacetic acid fragment (compounds **22a–g** for SAR in the planar acceptor pocket, Supporting Information: Table S2). New rounds of optimization included different substituents at the three position of the chlorophenyl ring of **22c** targeting the sulfonamide pocket, starting with sulfonamide moiety (compound **22j**, Supporting Information: Table S2). Subsequent improvements in potency were achieved leading to compound **22** with 95% KEAP1-NRF2 PPI inhibition at 15 nM measured by FP assay and a K_d value of 1.3 nM toward KEAP1 by ITC, being the most potent KEAP1-NRF2 PPI inhibitor described (compounds **22h–u** for SAR in the sulfonamide pocket, Supporting Information: Table S2). Cocrystal structures of several newly synthesized compounds with KEAP1 Kelch domain allowed authors to gain insights into its binding mode during the structure-driven process and confirmed expected interactions as predicted formerly in the initial hot spots. Together with its high affinity, compound **22** showed complementary interesting activities in both in vitro and in vivo experiments: (i) selectivity toward KEAP1 Kelch domain demonstrated in the GSK's enhanced cross-screen panel (eXP) containing 49 relevant targets; (ii) increased NRF2 nuclear translocation, and upregulated NRF2-dependent gene expression (NQO1 and GCLm) and NQO1 activity in normal human bronchial epithelial cells (NHBE); (iii) increased NQO1 activity in a human lung epithelial cell line (BEAS-2B) with an EC_{50} of 12 nM; (iv) prevented tertbutylhydroperoxide (tBHP)-induced glutathione depletion; (v) upregulated expression of NRF2-dependent genes (NQO1, thioredoxin reductase 1 [TXNRD1], GCLm, and HO-1) in COPD patient-derived bronchial epithelial cells; (vi) reduced disease advance in in vivo COPD models. In fact, intravenous (IV) infusion of compound **22** in rats led to an increased lung expression of NRF2-dependent genes (NQO1, HO-1, TXNRD1, SRXN1, GSTA3, and GCLc) and it attenuated ozone-induced pulmonary inflammation, reducing the accumulation of leukocytes in bronchoalveolar fluid and restoring GSH lung levels. In this model, rats were administered **22** by IV infusion over 6 and 24 h postdose they were exposed to ozone 1 ppm for 3 h.^{101,102}

Regarding promising results obtained with **22** in COPD-related models, Bewley et al.¹⁰³ reported that treatment with compound-induced expression of HO-1 in monocyte-derived macrophages (MDMs) and, importantly, GCLc and NQO1 in AM both from COPD patients. Moreover, **22** increased phagocytosis of opsonized and nonopsonized *S. pneumoniae* by COPD AMs and MDMs. In summary, this study reveals that COPD-induced systemic defects in phagocytosis and the more specific defect in phagocytosis of opsonized bacteria in AMs can be targeted with KEAP1-NRF2 PPI inhibitors.¹⁰³

3.2.4.1 | 1,4-Diphenyl-1,2,3-triazole core

A novel core structure with KEAP1-NRF2 PPI inhibitory capability was described by Wells group¹⁰⁴ from a docking-based virtual screening on KEAP1 structure (PDB-ID 2FLU) of ~178,000 molecules belonging to the ZINC clean fragments subset, that is, fragments without—even marginally—reactive functional groups.¹⁰⁵ Analysis of the top-ranking compounds revealed similarities in their binding mode within KEAP1 binding site, characterized by the establishment of electrostatic and hydrogen bond interactions between carboxylate or nitro substituents of the compounds and residues Arg380, Arg415, Arg483, and Asn382 of KEAP1, with further hydrogen bonds established

with Ser602 hydroxyl group for some compounds. This pharmacophore model was used to design a new family of 36 compounds based on a 1,4-diphenyl-1,2,3-triazole scaffold bearing a carboxylate, nitro, or carboxamide group in *meta* or *para* positions at both phenyl moieties (**23a–f**, Supporting Information: Table S2) aiming to maintain the interactions at P1 and P2 subpockets. The ability of these compounds to disrupt the KEAP1-NRF2 interaction was assessed via a competitive FP assay and further evaluated in a colorimetric NQO1 induction assay in Hepa1c1c7 cells. All compounds, except those bearing a *p*-carboxamide at 4-phenyl position, were able to disrupt the KEAP1-NRF2 interaction (32.0%–96.3%) at 100 μ M, being benzoic acid derivatives of remarkable potency. However, only six compounds showed NRF2 induction capacity in a cellular assay (**23b**, **23g**, **23h**, **23k**, **23l**, **23ax**; NQO1 expression >1.5-folds at 10 μ M). Carboxylate derivatives were inactive, being attributed to low cellular permeability. Based on the active 4-(*m*-nitrophenyl)-triazole scaffold, a new series of derivatives were obtained with different substituents at *meta* position of the 1-phenyl group (**23m–z**). Most of them showed good potency at FP and NQO1 induction assays ($IC_{50 (FP)} = 5.0 - 38.5 \mu M$, $CD_{NQO1} < 5 \mu M$). Compounds bearing a methyl (**23n**; $IC_{50 (FP)} = 10.0 \mu M$, $CD_{NQO1} = 1. \mu M$), chloride (**23w**; $IC_{50 (FP)} = 8.8 \mu M$, $CD_{NQO1} = 0.7 \mu M$), or iodine (**23**; $IC_{50 (FP)} = 7.1 \mu M$, $CD_{NQO1} = 0.6 \mu M$) substituent at *meta* position were the most active derivatives in both assays. Exposure of Hepa1c1c7 cells to a fixed 10 μ M concentration of **23n** and **23** for 24 h led to an increase of nuclear NRF2 and cytoplasmic HO-1 and NQO1 levels. Reversible binding of **22s** was demonstrated by means of a dialysis-based assay. Furthermore, disruption of KEAP1-NRF2 interaction by **23** was monitored in live cells using a TR-FRET-based assay system which suggested that **23** acts via disruption of KEAP1-DLG but not KEAP1-ETGE interaction.

Compound **23** was further identified as a mitophagy activator via p62 induction.^{106,107} In this line, MEF cells treated with **23** (10 μ M for 24 h) showed an increase in cytosolic and mitochondrial p62 protein levels accompanied by a reduction in mitochondrial network density and MTCO1 levels. Using the same conditions, authors also described an increase in mitochondrial LC3-II levels and LC3B mitochondrial colocalization. These effects were not observed in $p62^{-/-}$ and *NFE2L2* MEF cells, indicating that mitophagy induction by **23** is mediated by the NRF2/P62 pathway. Additionally, mitochondrial P62 colocalization and higher mitochondrial ubiquitination were also prompted by **23**. Interestingly, mitophagy activation was maintained in *Parkin* knockdown MEFs and in PINK1 knockout SH-SY5Y cells, indicating that **23** is able to trigger mitophagy even with a defective PINK1/Parkin pathway.¹⁰⁶ **23** treatment resulted in enhanced respiratory activity of mitochondria, as revealed by higher levels of mitochondrial superoxide radical and increased resting mitochondrial membrane potential.^{106,107} Superoxide overproduction was closely related to the mitophagy activation by **23** as cotreatment of MEF cells with **23** and mito-TEMPO, a specific mitochondrial superoxide radical scavenger, abolished LC3 mitochondrial localization prompted by treatment with **23** alone. Intriguingly, mitophagy was not triggered by covalent NRF2 inducers SFN, DMF, tert-butylhydroquinone, and curcumin, while nonelectrophilic **5**, **6**, **23**, and its analog compounds **23n** and **23ba** were all able to activate mitophagy.¹⁰⁷ Furthermore, **23n** exhibited neuroprotective activity against A β oligomer-induced toxicity.¹⁴ Treatment with **23n** significantly increased SH-SY5Y cells survival against 7PA2 CHO cell conditioned medium. This effect was indeed superior to the one exerted by the treatment with the electrophilic derivative bardoxolone-methyl when both compounds were used at their EC_{50} for NRF2 activation ($EC_{50} = 10 \mu M$ and $EC_{50} = 10 nM$ for **23n** and bardoxolone-methyl, respectively). Similarly, primary mouse neurons spine density loss upon Tg2576 conditioned media was rescued by **23n** treatment at 10 μ M.

3.2.5 | 1-Phenylpyrazole core

In 2017, Callahan et al. presented a patent application (GlaxoSmithKline and Astex Therapeutics) in which they reported a series of compounds based on a 1-biarylpyrazole scaffold as KEAP1-NRF2 PPI inhibitors (WO2017060854). Their activity was demonstrated in a competitive FP assay with a 16-mer ETGE peptide as well as by a TR-FRET assay using full-length KEAP1 and NRF2. These compounds were able to increase NQO1-specific activity following 48 h treatment in BEAS-2B cells. Among these molecules, compound **24**

(Table 2) showed the best overall activity (NQO1 activity induction $EC_{50} < 1$ nM, IC_{50} (FP) = 10–100 nM, IC_{50} (TR-FRET) < 10 nM). In 2018 they published a second patent on arylcyclohexyl-pyrazole-based compounds (WO2017060855A1). These compounds were also able to disrupt the KEAP1-NRF2 PPI and to augment NQO1-specific activity in BEAS-2B cells. Compound **25** (Table 2) exhibited the best overall activity (NQO1 activity induction $EC_{50} = 10$ –100 nM, IC_{50} (FP) = 10–100 nM, IC_{50} (TR-FRET) = 10–100 nM).

3.2.6 | Benzenesulfonyl-pyrimidone compounds

In addition to the discovery of compound **5** as one of the first KEAP1-NRF2 PPI inhibitors, Marcotte et al.¹¹⁶ also reported compound **26** from its HTS program (Table 2). Compared to **5**, compound **26** showed lower activity ($IC_{50} = 118$ μ M, FP assay) and failed to be active in the ARE-luciferase reporter assay in DLD1 cells. Interestingly, KEAP1 Kelch domain cocrystal structure revealed a 2:1 compound:protein binding stoichiometry side-by-side in the central cavity (PDB-ID **4IN4**). This binding mode was further verified by mass spectrometry and NMR experiments.¹¹⁶

3.2.7 | 3-(1,2,3,4-Tetrahydroisoquinolin-1-yl) propanoic acid compounds

Based on previous reports (compounds **5** and **26** from Marcotte et al.¹¹⁶), Ma et al.¹⁰⁸ designed new series of compounds testing their activity in an NRF2 nuclear translocation assay in the PathHunter U2OS KEAP1-NRF2 system. From this approach, they identified hit compound **27** ($EC_{50} = 0.95$ μ M for NRF2 translocation; K_d (SPR) = 56 nM for KEAP1 Kelch domain binding). Subsequent modifications at benzotriazole moiety led to compound **28** with improved affinity ($EC_{50} = 0.69$ μ M for NRF2 translocation; K_d (SPR) = 2.7 nM for KEAP1 Kelch domain binding). KEAP1 Kelch domain cocrystal structure (PDB-ID **6TYP**) revealed that compound **28** maintained important interactions with Arg415, Tyr525, and Ser602 as previously observed with compound **5**. Interestingly, it showed an additional strong interaction between its carboxylic acid moiety and Arg483 side chain. **28** was then submitted to SAR exploration around THIQ central core (compounds **28a–g** for SAR, Supporting Information: Table S2), and amide region (compounds **28h–o** for SAR, Supporting Information: Table S2). Second hit compound **29** was submitted to an additional SAR at the alpha position of carboxylic acid (compounds **29a–f** for SAR, Supporting Information: Table S2). Compound **29** achieved improved cellular activity and higher binding affinity ($EC_{50} = 0.36$ μ M for NRF2 translocation; K_d (SPR) = 0.7 nM for KEAP1 Kelch domain binding). **29** was extensively characterized showing no CYP isoenzyme inhibition at 10 μ M or hERG inhibition at 30 μ M, and good overall oral pharmacokinetic profile, however, it demonstrated low brain penetration, a result consistent with a high ER measured in MDCK-MDR1 cells. Other parameters like MDCK-MDR1 permeability, metabolic stability in human and rat liver microsomes, solubility, and free fraction of plasma protein binding, among others, were also evaluated. Furthermore, **29** was demonstrated to induce NRF2-dependent response (upregulated transcription of GCLC, oxidative stress-induced growth inhibitor 1 [OSGIN1], and NQO1; increased intracellular GSH levels with an $EC_{50} = 9.2$ nM) and prevent arsenite-induced death in human spinal cord astrocytes. Finally, target engagement evaluation in mice showed that **29** is able to increase NRF2-dependent genes expression in the kidney after a single oral dose (carbonyl reductase 3 (CBR3), NQO1, OSGIN1, and HO-1), however, it showed a slight upregulation of OSGIN1 levels in brain.¹⁰⁸

It is interesting to note that compound **29** assembles structural features of former 1,2,3,4-tetrahydroisoquinoline compounds and 3-phenylpropanoic acid compound **22**, which is one of the most promising KEAP1-NRF2 PPI inhibitors. Notwithstanding the above, there is not enough evidence for ensuring these compounds effectively disrupt KEAP1-NRF2 interaction. There are only KEAP1 binding data and crystallographic information, but there is a lack of competition experiments with NRF2.

3.2.8 | Ureas/hydrazinecarbohydrazide cores

Satoh et al.¹⁰⁹ performed a virtual screening using KEAP1-NRF2 complex structure (PDB-ID **2FLU**) combining commercially available molecules from ZINC database¹¹⁰ and an in-house library. Top-ranked compounds (65) were evaluated by SPR leading to the identification of 27 molecules that were active as KEAP1 binders. Among them, compound **30** (Table 2) was selected for further modifications to increase its KEAP1 affinity. The introduction of an oxyacetic group led to compound **31** (Table 2), described as a KEAP1-NRF2 PPI inhibitor, however, its affinity was not described. Surprisingly, the two crystal structures of KEAP1 with **31** (referred to as soaking and cocrystallized forms, PDB IDs **3VNH** and **3VNG**, respectively) revealed different binding modes depending on the method employed for the crystallization. 20 ns MD simulations of both complexes showed that the soaking form was more stable and thus considered to represent the biologically relevant interaction of **31** at the KEAP1 binding site.

Considering this type of derivatives, a closely related compound, **32** (Table 2), was previously reported as a potential KEAP1-NRF2 PPI inhibitor.¹¹¹ It showed NRF2 transcriptional activation in Huh-7.5 cells (CD = 1.36 μ M) and a dose-dependent KEAP1 binding measured by SPR (12.5–100 μ M). It also exerted protective effects against H₂O₂ cytotoxicity in Huh-7 cells. Moreover, **32** was evaluated in an in vivo rat model of diet-induced nonalcoholic steatohepatitis (NASH). Nine-week daily treatment with a low (20 mg/kg) or high (60 mg/kg) dose of **32** led to a reduction in the fibrosis score and in the liver fibrosis area. The antifibrotic effect of **32** was accompanied by a reduction in the carbonyl content of liver proteins evidencing its antioxidant effect. Furthermore, reduced liver damage was observed after treatment with **32**, as indicated by the lower plasma levels of aspartate and alanine aminotransferases. In addition, it was also able to reduce the progression of liver fibrosis when administrated only 4 weeks after 6 weeks of NASH-inducing diet, thus revealing a potential therapeutic effect.

In 2014, Sun et al.¹¹² performed a multistep virtual screening on KEAP1 based on compounds with negative formal charge at pH 7.4 extracted from the Specs database (21,199 molecules). After this initial filtering, a pharmacophore model was built based on the NRF2 ETGE peptide-KEAP1 interactions observed in crystallographic structures (PDB-ID **1X2R** and **2FLU**) and used as a second filtering stage. Docking of the remaining 2325 molecules led to the discovery of compound **33** (Table 2), which was able to disrupt KEAP1-NRF2 interaction (IC₅₀ (FP) = 9.80 μ M) and to activate the NRF2-ARE pathway in HEPG2-ARE-C8 cells. However, these compounds included acylhydrazone groups, which can be electrophilic under acidic conditions and can generate RNS after metabolism action.⁴⁵

3.2.9 | Pyrazolidine-3,5-dione, thiazolidine-2,4-dione, and 4-aminonaphthalen-1-ol compounds

Zhuang et al.¹¹³ reported some of the earliest noncovalent KEAP1-NRF2 PPI inhibitors. Authors performed a virtual screening of 153,611 compounds from the Specs database based on molecular docking using KEAP1 structure as target. Top 65 compounds from the screening were experimentally evaluated, nine of which showed inhibitory capacity at the low micromolar range. This effort led to the identification of three novel scaffolds exemplified by compounds **34** (IC₅₀ = 15.2 μ M), **35** (IC₅₀ = 10.4 μ M), and **36** (IC₅₀ = 2.9 μ M, Table 2). They performed then a hit-based substructure search (HBSS) again in Specs database with these novel scaffolds for subsequent SAR selecting derivatives: (i) Pyrazolidine-3,5-dione core from compound **34** (compounds **34a–e** for SAR, Supporting Information: Table S2); (ii) Thiazolidine-2,4-dione core from compound **35** (compounds **35a–e** for SAR, Supporting Information: Table S2); and (iii) 4-aminonaphthalen-1-ol core from compound **36** (compounds **36a–r** for SAR, Supporting Information: Table S2). Although potency of the initial hits was not improved, several novel derivatives were active at the low micromolar range such as **37** from the **36** scaffold bearing a triazole to carboxylic acid substitution (IC₅₀ = 4.2 μ M). The most potent derivatives of each class (**34**, **35**, **36**, and **37**) were then submitted to a reversibility study to verify their noncovalent binding to KEAP1. KEAP1 affinity was further assessed by differential

scanning fluorimetry (DSF) assay. Compound **36** showed a significant decrease in melting temperatures of KEAP1 protein (5°C), while **34** and **35** exhibited moderate potency (1 or 2°C). Moreover, compound **36** showed NRF2-dependant gene expression upregulation (HO-1 and NQO1) in rat adrenal gland PC12 cells, demonstrating also capacity to promote NRF2 nuclear localization.¹¹³ Considering the α,β -unsaturated carbonyl moiety of compounds **34** and **35** and the *p*-hydroxysulfonamide motif at **36**, which are susceptible of electrophilic reactivity or covalent adduct formation, authors explained that other compounds bearing this moiety in the SAR studies were not active in the FP assay, thus, this observation combined with reversibility experiments data suggests a noncovalent mechanism of action of these compounds.

Compound **36** was further optimized via an in-silico fragment growing process¹¹⁴ based on molecular docking studies to develop new derivatives bearing *N*-acetic or *N*-propionic acid moieties which were predicted to establish additional interactions in the KEAP1 pocket. Several benzenesulfonyl ring substitution patterns were evaluated (compounds **36s–ah** for SAR, Supporting Information: Table S2). Selected hit compounds **38** and **39** (Table 2) maintained low micromolar potency with a slight improvement in the case of derivative **38** compared to its parental compound **36** (IC_{50} = 1.14 μ M by FP assay; K_d = 453 nM by SPR for **38**; IC_{50} = 8.52 μ M; K_d = 5170 nM for **39**). Direct KEAP1 interaction of these compounds was assessed by DSF assay both showing increased values for melting temperature. At cellular level, efficacy of **38** and **39** was proven by different experiments: (i) they induced NRF2 nuclear translocation and upregulation of NRF2-dependent genes (HO-1 and NQO1) in rat H9c2 cardiac cells; (ii) they rescued H9c2 cells from LPS-challenge significantly restoring cell viability, decreasing ROS levels, and reducing LPS-induced secretion of pro-inflammatory cytokines such as TNF- α , IL-1 β , and IL-6. Additionally, **38** and **39** cardioprotective effects were determined in an in vivo mouse model of LPS-induced acute death. Both compounds led to an extended animal survival and reduced LPS-induced heart damage. NRF2 nuclear translocation and decreased levels of pro-inflammatory cytokines were also observed in mice heart tissue.¹¹⁴

Previously, Hu et al. reported (**WO2013067036**) an analog compound of the 4-aminonaphthalen-1-ol family, derivative **40** (**LH602**, Table 2). It was discovered in the FP-based screening of the NIH's molecular libraries probe production centers network library, which also led to the identification of compound **1**. **40** showed an IC_{50} value of 3 μ M measured by FP assay and a K_d value of 1.7 μ M to disrupt KEAP1-NRF2 interaction (SPR competition assay). Moreover, it was also evaluated in a cell-based ARE β -lactamase reporter assay exhibiting an EC_{50} value of 18 μ M being able to induce nuclear translocation of NRF2 in PathHunter U2OS KEAP1-NRF2 functional assay.

Finally, Jiang's group reported the last series of compounds belonging to the 4-aminonaphthalen-1-ol family (**WO2017124835**). In this case, they show a 2-oxy-2-phenylacetic acid substituted naphthalene sulfonamide. From a set of 20 derivatives, compound **41** was the most potent being also active in a cellular ARE-luciferase reporter assay (Table 2). This family was completed and published in a recent work¹²⁹ where authors performed an intensive SAR through this novel scaffold and they include further biological characterization for the hit compound **41** (compounds **41a–t** for SAR, Supporting Information: Table S2). Apart from its potency and strong binding affinity (IC_{50} = 75 nM by FP assay, K_d = 24.0 nM by ITC, and K_d = 36.5 nM by BLI), **41** activated NRF2 pathway in an ARE-luciferase reporter assay, induced NRF2 nuclear translocation and increased expression of downstream genes and proteins (HO-1, NQO1, and GCLm) in macrophage RAW 264.7 cells. Compound **41** also promoted the antioxidant capacity in these macrophage cells after LPS stimulus reducing ROS, restoring GSH/GSSG ratio, and increasing the expression of antioxidant enzymes such as SOD or GSHPx. Additionally, it antagonized the LPS-induced inflammatory conditions in both RAW 264.7 cells (decreased NO, IL-1b, IL-6, and TNF- α). Pharmacokinetic evaluation of **41** revealed that it was relatively stable when co-incubated with rat liver microsomes, it had no CYP isozyme inhibition at 10 μ M and it showed appropriate overall pharmacokinetic profile in rats.¹²⁹ Finally, in vivo evaluation of **41** in an LPS-induced systemic mouse model of inflammation demonstrated that it was able to decrease serum levels of IFN- γ , IL-1b, IL-6, and TNF- α .

3.2.10 | Iminocoumarin-benzothiazole compounds

Jiang et al.¹⁵ identified compound **42** (Table 2) as a new KEAP1-NRF2 PPI by means of a FP based screening of an in-house library of 569 compounds. **42** was able to bind to KEAP1 (K_d (SPR) = 48.1 μ M) and to inhibit the interaction between KEAP1 and a fluorescently labeled peptide in a competitive FP assay (K_d (FP) = 5.1 μ M). **42** increased nuclear NRF2 protein levels in H9c2 cardiac cells, prompting NRF2 translocation to the nucleus. NRF2 nuclear translocation was accompanied by an increase in NRF2-regulated genes HO-1 and NQO1 mRNA levels. In H9c2 cells treated with LPS, **42** was able to reduce pro-inflammatory cytokines TNF- α , IL-1 β , and IL-6 mRNA levels and to decrease ROS. Given the anti-inflammatory and antioxidant properties of **42** in vitro, authors further evaluated this compound in an in vivo model of septic cardiomyopathy, based on LPS treatment of C57BL/6 mice. Pretreatment with **42** for 12 h increased NRF2 levels in the left ventricular cells and reduced the mRNA levels of the pro-inflammatory cytokines TNF- α , IL-1 β , and IL-6 induced by LPS. **42** was also evaluated in an in vivo mouse model of hyperoxic acute lung injury, where it showed protective properties.¹³⁰ Treatment with **42** after exposure to hyperoxia-induced NRF2 and NRF2-related proteins in the lung reducing edema formation and neutrophil infiltration.

3.2.11 | N-(3-(1-H-Pyrazol-1-yl)phenyl)benzenesulfonamide compounds

Using an innovative approach, Pallesen et al.¹³¹ followed an alternative fragment-based deconstruction–reconstruction (FBDR) in the search of novel PPIs. In this case, known inhibitors were first deconstructed into fragments to generate a fragments library and then, after hit identification, reconstruction or merging of fragments was performed to obtain novel lead compounds. A set of six classes of known KEAP1-NRF2 PPI inhibitors for a total of 77 fragments was tested in four orthogonal assays: FP, thermal shift assay (TSA), saturation transfer difference (STD), NMR, and SPR. Thereafter, the most promising fragment hits were selected and characterized by X-ray crystallography towards KEAP1 Kelch domain binding. Merging two fragments hits assembled compound **43** with improved binding affinity showing IC_{50} = 15.6 μ M by FP assay and K_d = 2.9 μ M by SPR (Table 2). **43** was then submitted to a new optimization program resulting in 35 new derivatives, some of them with nanomolar activity (compounds **43a–aa** for SAR, Supporting Information: Table S2). Most promising modifications were combined to generate 18 new target compounds trying to either optimize the physicochemical properties or to enhance binding affinity (compounds **44a–r** for SAR, Supporting Information: Table S2). Combined aliphatic carboxylate and transcyclopropylbenzene derivatives showed the highest potency with IC_{50} FP values below or around 100 nM, exemplified by most potent compound **44** (Table 2). Additionally, key compounds **43**, **43l**, **43m**, **44a**, **44e**, **44i**, and **44** (Table 2, Supporting Information: Table S2) were metabolically stable in blood plasma and against mouse liver microsomes, however, they displayed very low permeabilities measured by PAMPA assay.¹³¹

3.2.12 | Natural products

Zhang et al.¹³² recently reported rutaecarpine (**45**, Table 2), a natural alkaloid isolated from *Evodia rutaecarpa*, with the ability to disrupt KEAP1-NRF2 interaction at 12.5 μ M by binding to KEAP1 (K_d (SPR) = 19.6 μ M). **45** increased NRF2 nuclear translocation in HCT116 and HepG2 cells as well as in primary mouse intestinal epithelial cells. Compound **45** also exhibited cytoprotective effects in HCT116 cells against H₂O₂-induced oxidative stress at a 5 μ M concentration. Treatment with **45** at an 80 mg/kg dose was also able to exert anti-inflammatory and protective effects in mouse model of DSS-induced colitis in an NRF2-dependent manner.

Gacesa et al.¹³³ reported two mycosporine-like aminoacids, **46** and **47** (Table 2), as KEAP1-NRF2 PPI inhibitors. Both compounds were able to disrupt KEAP1-NRF2 interaction, albeit with low potency (IC_{50} (FP assay) ~ 100 μ M)

and to bind KEAP1 Kelch domain as measured by DSF (**46** $\Delta T_m = 0.93^\circ\text{C}$; **47** $\Delta T_m = 0.64^\circ\text{C}$). Both compounds (100 μM for 24 h) induced NRF2 downstream genes after ultraviolet A radiation in 1BR cells.

Recently, Wu and coworkers¹³⁴ reported the marine carotenoid fucoxanthin (**48**, Table 2) extracted from seaweeds exerts neuroprotective effect via KEAP1-NRF2 PPI inhibition. BLI assays demonstrated that **48** is able to bind to KEAP1 ($K_d(\text{BLI}) = 51.6 \mu\text{M}$) and disrupt KEAP1-NRF2 PPI. In vitro studies in 6-OHDA-injured PC12 cells showed that **48** pretreatment induced NRF2 nuclear translocation, ARE activation, and increased the levels of the NRF2-driven HO-1, GCLm, and GCLc proteins. This activity translated into an antioxidant and antiapoptotic effect, as **48** pretreatment reduced ROS levels and the rates of early apoptosis, late apoptosis, and necrosis as well as the mitochondrial membrane depolarization caused by 6-OHDA. The neuroprotective potential of **48** was evaluated in vivo in zebrafish model of 6-OHDA-induced neurotoxicity. **48** pretreatment partially restored the 6-OHDA-prompted movement alteration, ROS levels, and brain granulosa disorder in a dose-dependent manner. The NRF2-ARE pathway activation by **48** was also observed in the zebrafish model, as mRNA levels of HO-1, GCLm, and GCLc were augmented by **48** treatment, while NRF2 and KEAP1 mRNA levels were not altered.

3.2.13 | Other compounds

Recently, Gorgulla et al.¹³⁵ developed an innovative VirtualFlow, an open-source virtual screening platform that allows virtual screening of chemical libraries in a large scale. To demonstrate the power of this platform, authors performed a virtual screening of 1.3 billion compounds (~1 billion belonging to the Enamine REAL library database and ~330 million from the ZINC15 library¹¹⁰) toward KEAP1 (PDB-ID **5FNQ**). Top 590 compounds were experimentally evaluated by a combination of SPR and NMR to assess their ability as KEAP1 binders as well as by competitive FP and BLI to evaluate their potential as KEAP1-NRF2 PPI inhibitors. Following this strategy, they identified 40 compounds that were able to bind to KEAP1 according to the SPR assay and to displace NRF2 peptide binding in FP and/or BLI. Removal of compounds containing PAINS, unsuitable for medicinal chemistry or that exhibited aggregation led to the final 13 hit compounds. FP-measured IC_{50} values of four of these compounds were reported: **49** ($\text{IC}_{50} = 0.258 \mu\text{M}$) **50** ($\text{IC}_{50} = 2.7 \mu\text{M}$), **51** ($\text{IC}_{50} = 38.2 \mu\text{M}$), and **52** ($\text{IC}_{50} = 14.2 \mu\text{M}$) (Table 2).

Kim et al.¹³⁶ identified compound **53** (Table 2) after performing a virtual screening of Asinex and Chemdiv chemical libraries using a ligand-based pharmacophore, structure-based pharmacophore, and docking combination strategy. **53** was able to inhibit KEAP1-NRF2 interaction in a pull-down assay and activate NRF2 nuclear translocation in cells ($\text{EC}_{50} = 1.46 \mu\text{M}$). BV-2 microglial and SH-SY5Y cells treatment with **53** increased NRF2 downstream proteins levels (GCLc, NQO1, and HO-1) in a dose-dependent manner. of BV-2 cells pretreatment with **53** exerted an anti-inflammatory effect after LPS stimulation, reducing iNOS, IL-1 β , and TNF- α levels as well as NO production. Cotreatment of LPS-stimulated BV-2 cells with NRF2 siRNA and **53** did not decrease NO production, thus demonstrating that the anti-inflammatory effect of this compound is exerted in an NRF2-dependent manner. Furthermore, **53** showed good BBB permeability (PAMPA-BBB assay) and 90.7% bioavailability via oral dosing and a $T_{1/2}$ of 1.2 h. Given the good pharmacokinetic profile of the compound, its potential therapeutic effect was assessed in vivo in an 1-methyl-4-phenyl-1,2,3,6-tetrahydropyridine (MPTP)-induced mouse model of Parkinson's disease (PD). Coadministration of **53** (30 mg/kg/day; 3 days; oral administration) with MPTP (20 mg/kg; four injections over 2 h) resulted reduced TH-positive dopaminergic neuron loss and decreased activated microglia (IBA1-positive) colocalization. Interestingly, it increased TH-positive neurons in the substantia nigra pars compacta at the end of the experiment (7 days). Furthermore, treatment with **53** alleviated motor impairment of the MPTP-injured mice in several motor activity tests (vertical grid, coat-hanger, and rotarod tests), thus demonstrating that NRF2 induction via KEAP1-NRF2 PPI inhibition by means of small molecules can be an effective therapeutic target for the treatment of PD.

Shimizu et al.¹³⁷ recently reported a new series of KEAP1-NRF2 PPI inhibitors identified by means of an LBVS strategy based on a machine-learning approach by generation of two random forest models. A PPI-oriented library

of ligands was used was chemical library. Selected compounds (620; 329 predicted as PPI-inhibitors and 291 randomly selected for comparison purposes) were then evaluated with a TR-FRET assay, which identified 15 hits that were able to disrupt KEAP1-NRF2 PPI to some extent at a 100 μM concentration, led by compounds **54** and **55** (85.5% and 74.3% of inhibition, respectively, Table 2).

Begnini et al.¹¹⁵ performed a virtual screening focused of 41 lead-like macrocycle-containing cores of natural products, which led to the identification of 5 different cores presumably able to bind to KEAP1. Given the synthetic complexity or reported cytotoxicity of four of these cores, only the cyclothialidine core was selected as the starting point for the development of new KEAP1-NRF2 PPI inhibitors (**56**, Table 2). Modifications on different regions of the core led to compound **56**, which was able to bind to KEAP1 ($K_{d(\text{ITC})} = 3.7 \mu\text{M}$) and was the most potent KEAP1-NRF2 PPI inhibitor among the evaluated compounds ($K_{d(\text{SPR})} = 4.1 \mu\text{M}$). Compound **56**-KEAP1 binding mode (PDB-ID **6Z6A**) shows that **56** binding is driven mainly by a cation- π interaction with Arg415, the establishment of a hydrogen bond with Ser602, and chloride-bridged hydrogen bonds with Asn382, Asn414, and Arg415. Furthermore, compound **56** was able to induce NRF2 nuclear translocation in cells (PathHunter U2OS Keap1-Nrf2 functional assay) at a 256 μM concentration. Assessment of drug-like properties of **56** showed that this compound had a high solubility aqueous solubility (805 μM in phosphate-buffer saline; $T = 25^\circ\text{C}$; $\text{pH} = 7.4$), moderate clearance in in vitro human liver microsomes ($\text{Cl}_{\text{int}} = 36.5 \mu\text{l/min/mg}$) and a relatively low passive permeability in an efflux-inhibited Caco-2 cell monolayer ($1.6 \times 10^{-6} \text{ cm/s}$).

Li and coworkers¹³⁸ reported a new class of KEAP1-NRF2 PPI inhibitors, based on rhodium (III) and iridium (III) metal complexes bearing bioactive ligands. Authors synthesized a series of novel derivatives which led to the identification of compound **57** as a potent NRF2-KEAP PPI inhibitor ($\text{IC}_{50}(\text{FP assay}) = 1.09 \mu\text{M}$) and KEAP1 binder ($K_{d(\text{ITC})} = 0.71 \mu\text{M}$). Moreover, compound **57** was able to induce NRF2 nuclear accumulation and to increase HO-1 and NQO1 protein levels in a KEAP1 and NRF2-dependent manner in LO2 cells. Then, the authors assessed the therapeutic potential of compound **57** against acetaminophen toxicity in this cell line, exhibiting a dose-dependent cytoprotective effect. Given the interesting properties of this compound, the authors evaluated its hepatoprotective ability in a mice model of acetaminophen-induced liver injury. Daily intraperitoneal administration of **57** (2.5 or 5.0 mg/kg) for 5 days previous to acetaminophen challenge was able to enhance NRF2 nuclear accumulation and NRF2-dependent proteins levels in the liver. Regarding its therapeutic effect, **57** treatment was able to reduce necrotic liver areas (21%–16% and 9% for low and high doses, respectively) and liver damage as reflected by aspartate and alanine aminotransferases serum levels (reduction of 23.5% and 25.2% following **57** low and high-dose treatments, respectively), thus compound **57** was able to exert a hepatoprotective effect in vivo presumably through NRF2 activation. Finally, the authors demonstrated that **57** mainly accumulates mainly in the liver and kidney without exerting organ damage or immunotoxicity.

4 | COMPARATIVE ASSESSMENT OF REPORTED KEAP1-NRF2 PPI INHIBITORS

In 2019, Tran and Pallesen et al.⁹⁵ reported a comparative assessment study in which they evaluated known KEAP1-NRF2 PPI compounds by FP, TSA, SPR, and cell activity NQO1 induction assay, among other assays. They resynthesized most important KEAP1-NRF2 PPI compounds reported to date and they discovered, surprisingly, that half of the compounds were inactive or they deviated substantially from its previously published activities. Significantly, these authors were not able to demonstrate reliable binding activity of compounds **23**, **31**, **32**, **33**, **34**, **35**, and **36**. Additionally, compounds **6**, **9**, **19**, and **22** were shown to be all high-affinity and cell-active compounds without any apparent chemical liabilities. This observation sustains that further work is needed in terms of assessing compound selectivity toward the KEAP1 Kelch domain, which has only been demonstrated for compounds **9** and **22**.⁹⁵

In view of the results and the discrepancies found for some of the published compounds, validation or reevaluation of the results might be required for some of the novel compounds. The development of KEAP1-NRF2 PPI inhibitors development of is a great challenge considering the difficulty of obtaining potent compounds with additional drug-like physicochemical properties and cell membrane permeability. For this reason, new compounds should be evaluated carefully and systematically by using different techniques to ensure the reliability of the results.

5 | CONCLUSIONS AND FUTURE PERSPECTIVES

The potential clinical application of NRF2 inducers has been widely described for different diseases with common pathophenotypes including exacerbated oxidative stress, chronic inflammation, and metabolic alterations.⁷ The discovery of novel therapeutic approaches able to up-regulate the KEAP1-NRF2-ARE pathway is an ever-increasing area since the approval of the first NRF2 inducer, DMF, for the treatment of multiple sclerosis. However, secondary undesired effects associated to electrophilic drug limited their clinical development. To overcome these limitations, increasing efforts are devoted to the development of innovative KEAP1-NRF2 PPI inhibitors, describing a wide number of novel chemical scaffolds able to disrupt the KEAP1-NRF2 interaction. Lead compounds have already demonstrated their capacity to induce NRF2 nuclear localization and NRF2-dependant genes expression in different in vitro and in vivo models. However, in many cases, highly polar peptides or small molecules were needed to interrupt this interaction, thus, limiting their development due to their low permeability across cell membranes. New efforts have included lead-to-drug optimizations directed to increase their permeability and to improve their pharmacokinetic properties, leading to highly promising drug candidates under development for different diseases.

The discovery of innovative KEAP1-NRF2 PPI inhibitors is a highly interesting alternative for the development of potentially safer NRF2 inducers with clinical applications. Current development has already demonstrated their capacity to interact at the KEAP1-NRF2 PPI interface and more importantly, their capacity to activate the phase II antioxidant response in many different cellular lines, increasing the expression of NRF2-dependent genes. Moreover, optimized compounds have also demonstrated beneficial effects in in vivo models of chronic inflammation (7), chronic ulcerative colitis (7, 45), retinal and cerebral ischemia (7), ALF (10, 57), steatohepatitis (32), LPS-induced toxicity (17, 38, 41, 42), acute lung injury (42), COPD (22), cardiac failure (21), AD (20), and PD (53, 48) demonstrating an extraordinary potential for the clinical application of this type of compounds. Considering chronic diseases, the use of noncovalent drugs might open a new therapeutic opportunity for these complex diseases that must be evaluated in the near future.

Although KEAP1-NRF2 PPI inhibitors overcome some of the limitations of the electrophilic or covalent modifiers NRF2 inducers, they could have some limitations regarding selectivity considering the KEAP1 interactome.^{139,140} As described, most KEAP1-NRF2 PPI inhibitors are designed to interact at the KEAP1 ETGE binding site, a place shared by different substrate proteins bearing an ETGE-like motif. That is, p62, a KEAP1 substrate able to interact to the ETGE motif, is known to activate the NRF2-ARE pathway, a capacity with many implications in cancer.⁹⁷ Noncanonical substrates include proteins such as AMER1 and FAM129B (both involved in the regulation of Wnt signaling), Nestin (neuron development), MCM3 (initiation of DNA replication), DPP3 (proteolysis), and SQSTM1 (autophagy). Although, in some cases, such additional interactions of PPI inhibitors would enhance their value by increasing complementary therapeutic actions, in other cases, these off-target effects could be deleterious. Thus, different scientists have proposed the development of drugs that interact with the KEAP1 DLGex binding site, seeking greater selectivity and avoiding side effects.¹³⁹ Additionally, the therapeutic window of NRF2 activation via KEAP1-NRF2 PPI inhibition should be taken into account in the development of these compounds. NRF2 hyperactivation has been related in several in vivo models to the development of bone hypoplasia.¹⁴¹ Hydronephrosis,¹⁴² esophagus, and forestomach hyperkeratosis¹⁴³ as well as altered mitochondrial bioenergetics, diabetes type 1 hallmarks, and aging acceleration.¹⁴⁴ Thus, although medicinal chemistry programs directed toward improving the potency of PPI inhibitors can be of great interest, main efforts should be focused on

improving their pharmacokinetic profile and a thorough assessment of their biological and safety profile. The therapeutic future of KEAP1-NRF2 PPI inhibitors is promising, although much work remains to be done.

ACKNOWLEDGMENTS

Enrique Crisman is the recipient of a PFIS fellowship of ISCIII. Pablo Duarte is the recipient of an FPU fellowship of the Spanish Ministry of education. Authors gratefully acknowledge funding from IS Carlos III, Comunidad de Madrid, and Spanish Research Agency. We thank Fundación Teófilo Hernando for its continued support. All schemes were created with [Biorender.com](https://biorender.com). IS Carlos III cofinanced by the European Regional Development funds (FEDER) grant number PI17/01700. General Council for Research and Innovation of the Community of Madrid and European Structural Funds (grant B2017/BMD-3827-NRF24ADCM. Spanish Ministry of Science, Innovation and Universities (grants PID2021-123481OB-I00, PID2021-122650OB-I00, PID2021-125986OB-I00, PDC2021-121421-I00, and PID2019-110061RB-I00). The authors have no financial support to disclose.

CONFLICT OF INTEREST

The authors declare no conflict of interest.

DATA AVAILABILITY STATEMENT

Data sharing not applicable to this article as no data sets were generated or analyzed during the current study.

ORCID

Maria Isabel Rodríguez-Franco  <http://orcid.org/0000-0002-6500-792X>

Rafael León  <http://orcid.org/0000-0003-4017-5756>

REFERENCES

1. Itoh K, Chiba T, Takahashi S, et al. An Nrf2/small Maf heterodimer mediates the induction of phase II detoxifying enzyme genes through antioxidant response elements. *Biochem Biophys Res Commun*. 1997;236(2):313-322.
2. Hayes JD, Dinkova-Kostova AT. The Nrf2 regulatory network provides an interface between redox and intermediary metabolism. *Trends Biochem Sci*. 2014;39(4):199-218.
3. Moi P, Chan K, Asunis I, Cao A, Kan YW. Isolation of NF-E2-related factor 2 (Nrf2), a NF-E2-like basic leucine zipper transcriptional activator that binds to the tandem NF-E2/AP1 repeat of the beta-globin locus control region. *Proc Natl Acad Sci U S A*. 1994;91(21):9926-9930.
4. Pajares M, Jiménez-Moreno N, García-Yagüe AJ, et al. Transcription factor NFE2L2/NRF2 is a regulator of macroautophagy genes. *Autophagy*. 2016;12(10):1902-1916.
5. Kobayashi A, Kang MI, Okawa H, et al. Oxidative stress sensor Keap1 functions as an adaptor for Cul3-based E3 ligase to regulate proteasomal degradation of Nrf2. *Mol Cell Biol*. 2004;24(16):7130-7139.
6. Cuadrado A, Rojo AI, Wells G, et al. Therapeutic targeting of the NRF2 and KEAP1 partnership in chronic diseases. *Nat Rev Drug Discov*. 2019;18(4):295-317.
7. Cuadrado A, Manda G, Hassan A, et al. Transcription factor NRF2 as a therapeutic target for chronic diseases: a systems medicine approach. *Pharmacol Rev*. 2018;70(2):348-383.
8. Buendia I, Michalska P, Navarro E, Gameiro I, Egea J, Leon R. Nrf2-ARE pathway: an emerging target against oxidative stress and neuroinflammation in neurodegenerative diseases. *Pharmacol Ther*. 2016;157:84-104.
9. Cuadrado A. NRF2 in neurodegenerative diseases. *Curr Opin Toxicol*. 2016;1:46-53.
10. Rojo de la Vega M, Chapman E, Zhang DD. NRF2 and the hallmarks of cancer. *Cancer Cell*. 2018;34(1):21-43.
11. Gazaryan IG, Thomas B. The status of Nrf2-based therapeutics: current perspectives and future prospects. *Neural Regen Res*. 2016;11(11):1708-1711.
12. Kaidery NA, Banerjee R, Yang L, et al. Targeting Nrf2-mediated gene transcription by extremely potent synthetic triterpenoids attenuate dopaminergic neurotoxicity in the MPTP mouse model of Parkinson's disease. *Antioxid Redox Signal*. 2013;18(2):139-157.
13. Lu MC, Zhao J, Liu YT, et al. CPUY192018, a potent inhibitor of the Keap1-Nrf2 protein-protein interaction, alleviates renal inflammation in mice by restricting oxidative stress and NF-kappaB activation. *Redox Biol*. 2019;26:101266.

14. Kerr F, Sofola-Adesakin O, Ivanov DK, et al. Direct Keap1-Nrf2 disruption as a potential therapeutic target for Alzheimer's disease. *PLoS Genet.* 2017;13(3):e1006593.
15. Jiang CS, Zhuang CL, Zhu K, et al. Identification of a novel small-molecule Keap1-Nrf2 PPI inhibitor with cytoprotective effects on LPS-induced cardiomyopathy. *J Enzyme Inhib Med Chem.* 2018;33(1):833-841.
16. Sies H, Berndt C, Jones DP. Oxidative stress. *Annu Rev Biochem.* 2017;86:715-748.
17. MacLeod AK, McMahon M, Plummer SM, et al. Characterization of the cancer chemopreventive NRF2-dependent gene battery in human keratinocytes: demonstration that the KEAP1-NRF2 pathway, and not the BACH1-NRF2 pathway, controls cytoprotection against electrophiles as well as redox-cycling compounds. *Carcinogenesis.* 2009;30(9):1571-1580.
18. McMahon M, Itoh K, Yamamoto M, et al. The Cap'n'Collar basic leucine zipper transcription factor Nrf2 (NF-E2 p45-related factor 2) controls both constitutive and inducible expression of intestinal detoxification and glutathione biosynthetic enzymes. *Cancer Res.* 2001;61(8):3299-3307.
19. Thimmulappa RK, Mai KH, Srisuma S, Kensler TW, Yamamoto M, Biswal S. Identification of Nrf2-regulated genes induced by the chemopreventive agent sulforaphane by oligonucleotide microarray. *Cancer Res.* 2002;62(18):5196-5203.
20. Aleksunes LM, Manautou JE. Emerging role of Nrf2 in protecting against hepatic and gastrointestinal disease. *Toxicol Pathol.* 2007;35(4):459-473.
21. Ma Q. Role of nrf2 in oxidative stress and toxicity. *Annu Rev Pharmacol Toxicol.* 2013;53:401-426.
22. Mittal M, Siddiqui MR, Tran K, Reddy SP, Malik AB. Reactive oxygen species in inflammation and tissue injury. *Antioxid Redox Signaling.* 2014;20(7):1126-1167.
23. Wardyn JD, Ponsford AH, Sanderson CM. Dissecting molecular cross-talk between Nrf2 and NF- κ B response pathways. *Biochem Soc Trans.* 2015;43(4):621-626.
24. Kim JE, You DJ, Lee C, Ahn C, Seong JY, Hwang JI. Suppression of NF-kappaB signaling by KEAP1 regulation of IKKbeta activity through autophagic degradation and inhibition of phosphorylation. *Cellular Signalling.* 2010;22(11):1645-1654.
25. Liu GH, Qu J, Shen X. NF-kappaB/p65 antagonizes Nrf2-ARE pathway by depriving CBP from Nrf2 and facilitating recruitment of HDAC3 to MafK. *Biochem Biophys Acta.* 2008;1783(5):713-727.
26. Sun Z, Chin YE, Zhang DD. Acetylation of Nrf2 by p300/CBP augments promoter-specific DNA binding of Nrf2 during the antioxidant response. *Mol Cell Biol.* 2009;29(10):2658-2672.
27. Sheedy FJ, Grebe A, Rayner KJ, et al. CD36 coordinates NLRP3 inflammasome activation by facilitating intracellular nucleation of soluble ligands into particulate ligands in sterile inflammation. *Nature Immunol.* 2013;14(8):812-820.
28. Kobayashi EH, Suzuki T, Funayama R, et al. Nrf2 suppresses macrophage inflammatory response by blocking proinflammatory cytokine transcription. *Nat Commun.* 2016;7:11624.
29. Pajares M, Rojo AI, Arias E, Díaz-Carretero A, Cuervo AM, Cuadrado A. Transcription factor NFE2L2/NRF2 modulates chaperone-mediated autophagy through the regulation of LAMP2A. *Autophagy.* 2018;14(8):1310-1322.
30. Scrivo A, Bourdenx M, Pampliega O, Cuervo AM. Selective autophagy as a potential therapeutic target for neurodegenerative disorders. *Lancet Neurol.* 2018;17(9):802-815.
31. Katsuragi Y, Ichimura Y, Komatsu M. Regulation of the Keap1-Nrf2 pathway by p62/SQSTM1. *Curr Opin Toxicol.* 2016;1:54-61.
32. Zhu L, He S, Huang L, et al. Chaperone-mediated autophagy degrades Keap1 and promotes Nrf2-mediated antioxidative response. *Aging Cell.* 2022;21(6):e13616.
33. McMahon M, Thomas N, Itoh K, Yamamoto M, Hayes JD. Redox-regulated turnover of Nrf2 is determined by at least two separate protein domains, the redox-sensitive Neh2 degon and the redox-insensitive Neh6 degon. *J Biol Chem.* 2004;279(30):31556-31567.
34. Tong KI, Katoh Y, Kusunoki H, Itoh K, Tanaka T, Yamamoto M. Keap1 recruits Neh2 through binding to ETGE and DLG motifs: characterization of the two-site molecular recognition model. *Mol Cell Biol.* 2006;26(8):2887-2900.
35. Chowdhry S, Zhang Y, McMahon M, Sutherland C, Cuadrado A, Hayes JD. Nrf2 is controlled by two distinct β -TrCP recognition motifs in its Neh6 domain, one of which can be modulated by GSK-3 activity. *Oncogene.* 2013;32(32):3765-3781.
36. Canning P, Sorrell FJ, Bullock AN. Structural basis of Keap1 interactions with Nrf2. *Free Radic Biol Med.* 2015; 88(Pt B):101-107.
37. Dinkova-Kostova AT, Holtzclaw WD, Cole RN, et al. Direct evidence that sulfhydryl groups of Keap1 are the sensors regulating induction of phase 2 enzymes that protect against carcinogens and oxidants. *Proc Natl Acad Sci U S A.* 2002;99(18):11908-11913.
38. Zhang DD, Hannink M. Distinct cysteine residues in Keap1 are required for Keap1-dependent ubiquitination of Nrf2 and for stabilization of Nrf2 by chemopreventive agents and oxidative stress. *Mol Cell Biol.* 2003;23(22):8137-8151.

39. Tong KI, Kobayashi A, Katsuoka F, Yamamoto M. Two-site substrate recognition model for the Keap1-Nrf2 system: a hinge and latch mechanism. *Biol Chem*. 2006;387(10-11):1311-1320.
40. Cleasby A, Yon J, Day PJ, et al. Structure of the BTB domain of Keap1 and its interaction with the triterpenoid antagonist CDDO. *PLoS One*. 2014;9(6):e98896.
41. Horie Y, Suzuki T, Inoue J, et al. Molecular basis for the disruption of Keap1-Nrf2 interaction via Hinge & Latch mechanism. *Commun Biol*. 2021;4(1):576.
42. Egger AL, Small E, Hannink M, Mesecar AD. Cul3-mediated Nrf2 ubiquitination and antioxidant response element (ARE) activation are dependent on the partial molar volume at position 151 of Keap1. *Biochem J*. 2009;422(1):171-180.
43. Rachakonda G, Xiong Y, Sekhar KR, Stamer SL, Liebler DC, Freeman ML. Covalent modification at Cys151 dissociates the electrophile sensor Keap1 from the ubiquitin ligase CUL3. *Chem Res Toxicol*. 2008;21(3):705-710.
44. Baird L, Swift S, Lières D, Dinkova-Kostova AT. Monitoring Keap1-Nrf2 interactions in single live cells. *Biotech Adv*. 2014;32(6):1133-1144.
45. Pallesen JS, Tran KT, Bach A. Non-covalent small-molecule Kelch-like ECH-Associated protein 1-nuclear factor erythroid 2-related factor 2 (Keap1-Nrf2) inhibitors and their potential for targeting central nervous system diseases. *J Med Chem*. 2018;61(18):8088-8103.
46. DeNicola GM, Karreth FA, Humpton TJ, et al. Oncogene-induced Nrf2 transcription promotes ROS detoxification and tumorigenesis. *Nature*. 2011;475(7354):106-109.
47. Kwak MK, Itoh K, Yamamoto M, Kensler TW. Enhanced expression of the transcription factor Nrf2 by cancer chemopreventive agents: role of antioxidant response element-like sequences in the nrf2 promoter. *Mol Cell Biol*. 2002;22(9):2883-2892.
48. Yu S, Khor TO, Cheung KL, et al. Nrf2 expression is regulated by epigenetic mechanisms in prostate cancer of TRAMP mice. *PLoS One*. 2010;5(1):e8579.
49. Brennan MS, Matos MF, Li B, et al. Dimethyl fumarate and monoethyl fumarate exhibit differential effects on KEAP1, NRF2 activation, and glutathione depletion in vitro. *PLoS One*. 2015;10(3):e0120254.
50. Linker RA, Lee DH, Ryan S, et al. Fumaric acid esters exert neuroprotective effects in neuroinflammation via activation of the Nrf2 antioxidant pathway. *Brain*. 2011;134(Pt 3):678-692.
51. Zheng S, Santosh Laxmi YR, David E, et al. Synthesis, chemical reactivity as Michael acceptors, and biological potency of monocyclic cyanoenones, novel and highly potent anti-inflammatory and cytoprotective agents. *J Med Chem*. 2012;55(10):4837-4846.
52. Rojo AI, Rada P, Mendiola M, et al. The PTEN/NRF2 axis promotes human carcinogenesis. *Antioxid Redox Signal*. 2014;21(18):2498-2514.
53. Casares L, Moreno R, Ali KX, et al. The synthetic triterpenoids CDDO-TFEA and CDDO-Me, but not CDDO, promote nuclear exclusion of BACH1 impairing its activity. *Redox Biol*. 2022;51:102291.
54. Gillard GO, Collette B, Anderson J, et al. DMF, but not other fumarates, inhibits NF-kappaB activity in vitro in an Nrf2-independent manner. *J Neuroimmunol*. 2015;283:74-85.
55. Attucks OC, Jasmer KJ, Hannink M, et al. Induction of heme oxygenase I (HMOX1) by HPP-4382: a novel modulator of Bach1 activity. *PLoS One*. 2014;9(7):e101044.
56. Singh A, Venkannagari S, Oh KH, et al. Small molecule inhibitor of NRF2 selectively intervenes therapeutic resistance in KEAP1-deficient NSCLC tumors. *ACS Chem Biol*. 2016;11(11):3214-3225.
57. The PyMOL Molecular Graphics System, Schrödinger, LLC. [computer program]. Version 2.0; 2022.
58. Canning P, Cooper CDO, Krojer T, et al. Structural basis for Cul3 protein assembly with the BTB-Kelch family of E3 ubiquitin ligases. *J Biol Chem*. 2013;288(11):7803-7814.
59. Lo SC, Li X, Henzl MT, Beamer LJ, Hannink M. Structure of the Keap1:Nrf2 interface provides mechanistic insight into Nrf2 signaling. *EMBO J*. 2006;25(15):3605-3617.
60. Fukutomi T, Takagi K, Mizushima T, Ohuchi N, Yamamoto M. Kinetic, thermodynamic, and structural characterizations of the association between Nrf2-DLGex degron and Keap1. *Mol Cell Biol*. 2014;34(5):832-846.
61. Padmanabhan B, Tong KI, Ohta T, et al. Structural basis for defects of Keap1 activity provoked by its point mutations in lung cancer. *Mol Cell*. 2006;21(5):689-700.
62. Tong KI, Padmanabhan B, Kobayashi A, et al. Different electrostatic potentials define ETGE and DLG motifs as hinge and latch in oxidative stress response. *Mol Cell Biol*. 2007;27(21):7511-7521.
63. Leung CH, Zhang JT, Yang GJ, Liu H, Han QB, Ma DL. Emerging screening approaches in the development of Nrf2-Keap1 protein-protein interaction inhibitors. *Int J Mol Sci*. 2019;20(18):4445.
64. Mou Y, Wen S, Li YX, Gao XX, Zhang X, Jiang ZY. Recent progress in Keap1-Nrf2 protein-protein interaction inhibitors. *Eur J Med Chem*. 2020;202:112532.
65. Lee S, Hu L. Nrf2 activation through the inhibition of Keap1-Nrf2 protein-protein interaction. *Med Chem Res*. 2020;29(5):846-867.

66. Nevola L, Giralt E. Modulating protein-protein interactions: the potential of peptides. *Chem Commun (Camb)*. 2015;51(16):3302-3315.
67. Smith MC, Gestwicki JE. Features of protein-protein interactions that translate into potent inhibitors: topology, surface area and affinity. *Expert Rev Mol Med*. 2012;14:e16.
68. Cunningham AD, Qvit N, Mochly-Rosen D. Peptides and peptidomimetics as regulators of protein-protein interactions. *Curr Opin Struct Biol*. 2017;44:59-66.
69. Inoyama D, Chen Y, Huang X, Beamer LJ, Kong AN, Hu L. Optimization of fluorescently labeled Nrf2 peptide probes and the development of a fluorescence polarization assay for the discovery of inhibitors of Keap1-Nrf2 interaction. *J Biomol Screening*. 2012;17(4):435-447.
70. Hancock R, Bertrand HC, Tsujita T, et al. Peptide inhibitors of the Keap1-Nrf2 protein-protein interaction. *Free Radic Biol Med*. 2012;52(2):444-451.
71. Lu M-C, Chen Z-Y, Wang Y-L, et al. Binding thermodynamics and kinetics guided optimization of potent Keap1-Nrf2 peptide inhibitors. *RSC Adv*. 2015;5(105):85983-85987.
72. Chen Y, Inoyama D, Kong AN, Beamer LJ, Hu L. Kinetic analyses of Keap1-Nrf2 interaction and determination of the minimal Nrf2 peptide sequence required for Keap1 binding using surface plasmon resonance. *Chem Biol Drug Des*. 2011;78(6):1014-1021.
73. Hancock R, Schaap M, Pfister H, Wells G. Peptide inhibitors of the Keap1-Nrf2 protein-protein interaction with improved binding and cellular activity. *Org Biomol Chem*. 2013;11(21):3553-3557.
74. Georgakopoulos ND, Talapatra SK, Gatliff J, Kozielski F, Wells G. Modified peptide inhibitors of the Keap1-Nrf2 protein-protein interaction incorporating unnatural amino acids. *Chembiochem*. 2018;19(17):1810-1816.
75. Colarusso S, De Simone D, Frattarelli T, et al. Optimization of linear and cyclic peptide inhibitors of KEAP1-NRF2 protein-protein interaction. *Bioorg Med Chem*. 2020;28(21):115738.
76. Lu MC, Jiao Q, Liu T, et al. Discovery of a head-to-tail cyclic peptide as the Keap1-Nrf2 protein-protein interaction inhibitor with high cell potency. *Eur J Med Chem*. 2018;143:1578-1589.
77. Salim H, Song J, Sahni A, Pei D. Development of a cell-permeable cyclic peptidyl inhibitor against the Keap1-Nrf2 interaction. *J Org Chem*. 2020;85(3):1416-1424.
78. Steel RJ, O'Connell MA, Searcey M. Perfluoroarene-based peptide macrocycles that inhibit the Nrf2/Keap1 interaction. *Bioorg Med Chem Lett*. 2018;28(16):2728-2731.
79. Chen K, Huang L, Shen B. Rational cyclization-based minimization of entropy penalty upon the binding of Nrf2-derived linear peptides to Keap1: a new strategy to improve therapeutic peptide activity against sepsis. *Biophys Chem*. 2019;244:22-28.
80. Steel R, Cowan J, Payerne E, O'Connell MA, Searcey M. Anti-inflammatory effect of a cell-penetrating peptide targeting the Nrf2/Keap1 interaction. *ACS Med Chem Lett*. 2012;3(5):407-410.
81. Owens AE, Iannuzzelli JA, Gu Y, Fasan R. MORPH-PhD: an integrated phage display platform for the discovery of functional genetically encoded peptide macrocycles. *ACS Cent Sci*. 2020;6(3):368-381.
82. Li L, Liu J, Nie S, et al. Direct inhibition of Keap1-Nrf2 interaction by egg-derived peptides DKK and DDW revealed by molecular docking and fluorescence polarization. *RSC Adv*. 2017;7(56):34963-34971.
83. Sogabe S, Sakamoto K, Kamada Y, Kadotani A, Fukuda Y, Sakamoto JI. Discovery of a Kelch-like ECH-associated protein 1-inhibitory tetrapeptide and its structural characterization. *Biochem Biophys Res Commun*. 2017;486(3):620-625.
84. Zhao J, Redell JB, Moore AN, Dash PK. A novel strategy to activate cytoprotective genes in the injured brain. *Biochem Biophys Res Commun*. 2011;407(3):501-506.
85. Tu J, Zhang X, Zhu Y, et al. Cell-permeable peptide targeting the Nrf2-Keap1 interaction: a potential novel therapy for global cerebral ischemia. *J Neurosci*. 2015;35(44):14727-14739.
86. Hu L, Magesh S, Chen L, et al. Discovery of a small-molecule inhibitor and cellular probe of Keap1-Nrf2 protein-protein interaction. *Bioorg Med Chem Lett*. 2013;23(10):3039-3043.
87. Wang L, Lewis T, Zhang YL, et al. The identification and characterization of non-reactive inhibitor of Keap1-Nrf2 interaction through HTS using a fluorescence polarization assay. *Probe Reports from the NIH Molecular Libraries Program*. National Center for Biotechnology Information; 2010.
88. Wen X, Thorne G, Hu L, Joy MS, Aleksunes LM. Activation of NRF2 signaling in HEK293 cells by a first-in-class direct KEAP1-NRF2 inhibitor. *J Biochem Mol Toxicol*. 2015;29(6):261-266.
89. Jnoff E, Albrecht C, Barker JJ, et al. Binding mode and structure-activity relationships around direct inhibitors of the Nrf2-Keap1 complex. *ChemMedChem*. 2014;9(4):699-705.
90. Ontoria JM, Biancofiore I, Fezzardi P, et al. Combined peptide and small-molecule approach toward nonacidic THIQ inhibitors of the KEAP1/NRF2 interaction. *ACS Med Chem Lett*. 2020;11(5):740-746.
91. Jiang ZY, Lu MC, Xu LL, et al. Discovery of potent Keap1-Nrf2 protein-protein interaction inhibitor based on molecular binding determinants analysis. *J Med Chem*. 2014;57(6):2736-2745.

92. Lu M-C, Tan S-J, Ji J-A, et al. Polar recognition group study of Keap1-Nrf2 protein-protein interaction inhibitors. *ACS Med Chem Lett.* 2016;7(9):835-840.
93. Lazzara PR, David BP, Ankireddy A, et al. Isoquinoline Kelch-like ECH-Associated protein 1-nuclear factor (erythroid-derived 2)-like 2 (KEAP1-NRF2) inhibitors with high metabolic stability. *J Med Chem.* 2019;63:6547-6560.
94. Lazzara PR, Jain AD, Maldonado AC, et al. Synthesis and evaluation of noncovalent naphthalene-based KEAP1-NRF2 inhibitors. *ACS Med Chem Lett.* 2020;11(4):521-527.
95. Tran KT, Pallesen JS, Solbak S, et al. A comparative assessment study of known small-molecule Keap1-Nrf2 protein-protein interaction inhibitors: chemical synthesis, binding properties, and cellular activity. *J Med Chem.* 2019;62(17):8028-8052.
96. Abed DA, Lee S, Hu L. Discovery of disubstituted xylene derivatives as small molecule direct inhibitors of Keap1-Nrf2 protein-protein interaction. *Bioorg Med Chem.* 2020;28(6):115343.
97. Saito T, Ichimura Y, Taguchi K, et al. p62/Sqstm1 promotes malignancy of HCV-positive hepatocellular carcinoma through Nrf2-dependent metabolic reprogramming. *Nat Commun.* 2016;7:12030.
98. Lu MC, Ji JA, Jiang YL, et al. An inhibitor of the Keap1-Nrf2 protein-protein interaction protects NCM460 colonic cells and alleviates experimental colitis. *Sci Rep.* 2016;6:26585.
99. Hui Q, Karlstetter M, Xu Z, et al. Inhibition of the Keap1-Nrf2 protein-protein interaction protects retinal cells and ameliorates retinal ischemia-reperfusion injury. *Free Radic Biol Med.* 2020;146:181-188.
100. Zhou HS, Hu LB, Zhang H, et al. Design, synthesis, and structure-activity relationships of indoline-based Kelch-like ECH-associated protein 1-nuclear factor (erythroid-derived 2)-like 2 (Keap1-Nrf2) protein-protein interaction inhibitors. *J Med Chem.* 2020;63(19):11149-11168.
101. Davies TG, Wixted WE, Coyle JE, et al. Monoacidic inhibitors of the Kelch-like ECH-associated protein 1: nuclear factor erythroid 2-Related factor 2 (KEAP1:NRF2) protein-protein interaction with high cell potency identified by fragment-based discovery. *J Med Chem.* 2016;59(8):3991-4006.
102. Heightman TD, Callahan JF, Chiarparin E, et al. Structure-activity and structure-conformation relationships of aryl propionic acid inhibitors of the kelch-like ECH-associated protein 1/nuclear factor erythroid 2-related factor 2 (KEAP1/NRF2) protein-protein interaction. *J Med Chem.* 2019;62(9):4683-4702.
103. Bewley MA, Budd RC, Ryan E, et al. Opsonic phagocytosis in chronic obstructive pulmonary disease is enhanced by Nrf2 agonists. *Am J Respir Crit Care Med.* 2018;198(6):739-750.
104. Bertrand HC, Schaap M, Baird L, et al. Design, synthesis, and evaluation of triazole derivatives that induce Nrf2 dependent gene products and inhibit the Keap1-Nrf2 protein-protein interaction. *J Med Chem.* 2015;58(18):7186-7194.
105. Irwin JJ, Sterling T, Mysinger MM, Bolstad ES, Coleman RG. ZINC: a free tool to discover chemistry for biology. *J Chem Inf Model.* 52, 2012:1757-1768.
106. East DA, Fagiani F, Crosby J, et al. PMI: a $\Delta\psi$ m independent pharmacological regulator of mitophagy. *Chem Biol.* 2014;21(11):1585-1596.
107. Georgakopoulos ND, Frison M, Alvarez MS, Bertrand H, Wells G, Campanella M. Reversible Keap1 inhibitors are preferential pharmacological tools to modulate cellular mitophagy. *Sci Rep.* 2017;7(1):10303.
108. Ma B, Lucas B, Capacci A, et al. Design, synthesis and identification of novel, orally bioavailable non-covalent Nrf2 activators. *Bioorg Med Chem Lett.* 2020;30(4):126852.
109. Satoh M, Saburi H, Tanaka T, et al. Multiple binding modes of a small molecule to human Keap1 revealed by X-ray crystallography and molecular dynamics simulation. *FEBS Open Bio.* 2015;5:557-570.
110. Sterling T, Irwin JJ. ZINC 15--Ligand discovery for everyone. *J Chem Inf Model.* 2015;55(11):2324-2337.
111. Shimozone R, Asaoka Y, Yoshizawa Y, et al. Nrf2 activators attenuate the progression of nonalcoholic steatohepatitis-related fibrosis in a dietary rat model. *Mol Pharmacol.* 2013;84(1):62-70.
112. Sun H-P, Jiang Z-Y, Zhang M-Y, et al. Novel protein-protein interaction inhibitor of Nrf2-Keap1 discovered by structure-based virtual screening. *MedChemComm.* 2014;5(1):93-98.
113. Zhuang C, Narayanapillai S, Zhang W, Sham YY, Xing C. Rapid identification of Keap1-Nrf2 small-molecule inhibitors through structure-based virtual screening and hit-based substructure search. *J Med Chem.* 2014;57(3):1121-1126.
114. Meng N, Tang H, Zhang H, et al. Fragment-growing guided design of Keap1-Nrf2 protein-protein interaction inhibitors for targeting myocarditis. *Free Radic Biol Med.* 2018;117:228-237.
115. Begnini F, Poongavanam V, Over B, et al. Mining natural products for macrocycles to drug difficult targets. *J Med Chem.* 2021;64(2):1054-1072.
116. Marcotte D, Zeng W, Hus JC, et al. Small molecules inhibit the interaction of Nrf2 and the Keap1 Kelch domain through a non-covalent mechanism. *Bioorg Med Chem.* 2013;21(14):4011-4019.
117. Wang L, Chen X, Li X, et al. Developing a novel strategy for COPD therapy by targeting Nrf2 and metabolism reprogramming simultaneously. *Free Radic Biol Med.* 2021;169:436-445.

118. Jiang ZY, Xu LL, Lu MC, et al. Structure-activity and structure-property relationship and exploratory in vivo evaluation of the nanomolar Keap1-Nrf2 protein-protein interaction inhibitor. *J Med Chem*. 2015;58(16):6410-6421.
119. Winkel AF, Engel CK, Margerie D, et al. Characterization of RA839, a noncovalent small molecule binder to Keap1 and selective activator of Nrf2 signaling. *J Biol Chem*. 2015;290(47):28446-28455.
120. Lu MC, Zhang X, Wu F, et al. Discovery of a potent Kelch-Like ECH-associated protein 1-Nuclear factor erythroid 2-related factor 2 (Keap1-Nrf2) protein-protein interaction inhibitor with natural proline structure as a cytoprotective agent against acetaminophen-induced hepatotoxicity. *J Med Chem*. 2019;62(14):6796-6813.
121. Jain AD, Potteti H, Richardson BG, et al. Probing the structural requirements of non-electrophilic naphthalene-based Nrf2 activators. *Eur J Med Chem*. 2015;103:252-268.
122. Richardson BG, Jain AD, Potteti HR, et al. Replacement of a naphthalene scaffold in kelch-like ECH-associated protein 1 (KEAP1)/nuclear factor (erythroid-derived 2)-like 2 (NRF2) inhibitors. *J Med Chem*. 2018;61(17):8029-8047.
123. Lu M, Zhang X, Zhao J, You Q, Jiang Z. A hydrogen peroxide responsive prodrug of Keap1-Nrf2 inhibitor for improving oral absorption and selective activation in inflammatory conditions. *Redox Biol*. 2020;34:101565.
124. Yasuda D, Nakajima M, Yuasa A, et al. Synthesis of Keap1-phosphorylated p62 and Keap1-Nrf2 protein-protein interaction inhibitors and their inhibitory activity. *Bioorg Med Chem Lett*. 2016;26(24):5956-5959.
125. Yasuda D, Ohe T, Takahashi K, et al. Inhibitors of the protein-protein interaction between phosphorylated p62 and Keap1 attenuate chemoresistance in a human hepatocellular carcinoma cell line. *Free Radic Res*. 2020;54:1-13.
126. Yasuda D, Yuasa A, Obata R, et al. Discovery of benzo[g]indoles as a novel class of non-covalent Keap1-Nrf2 protein-protein interaction inhibitor. *Bioorg Med Chem Lett*. 2017;27(22):5006-5009.
127. Lu M, Zhou HS, You QD, Jiang Z. Design, synthesis, and initial evaluation of affinity-based small-molecule probes for fluorescent visualization and specific detection of Keap1. *J Med Chem*. 2016;59(15):7305-7310.
128. Sun Y, Huang J, Chen Y, et al. Direct inhibition of Keap1-Nrf2 protein-protein interaction as a potential therapeutic strategy for Alzheimer's disease. *Bioorg Chem*. 2020;103:104172.
129. Lu MC, Shao HL, Liu T, You QD, Jiang ZY. Discovery of 2-oxy-2-phenylacetic acid substituted naphthalene sulfonamide derivatives as potent KEAP1-NRF2 protein-protein interaction inhibitors for inflammatory conditions. *Eur J Med Chem*. 2020;207:112734.
130. Wan J, Lin S, Huang X, Li Q, Zeng L, Du S. ZJ01, a small molecule inhibitor of the Kelch-like ECH-associated protein 1-nuclear factor erythroid 2-related factor 2 (Keap1-Nrf2) protein-protein interaction, reduces hyperoxic acute lung injury in a mouse model. *Med Sci Monit*. 2020;26:e920467.
131. Pallesen JS, Narayanan D, Tran KT, et al. Deconstructing noncovalent kelch-like ECH-associated protein 1 (Keap1) inhibitors into fragments to reconstruct new potent compounds. *J Med Chem*. 2021;64(8):4623-4661.
132. Zhang Y, Yan T, Sun D, et al. Rutaecarpine inhibits KEAP1-NRF2 interaction to activate NRF2 and ameliorate dextran sulfate sodium-induced colitis. *Free Radic Biol Med*. 2020;148:33-41.
133. Gacesa R, Lawrence KP, Georgakopoulos ND, et al. The mycosporine-like amino acids porphyra-334 and shinorine are antioxidants and direct antagonists of Keap1-Nrf2 binding. *Biochimie*. 2018;154:35-44.
134. Wu W, Han H, Liu J, et al. Fucoxanthin prevents 6-OHDA-induced neurotoxicity by targeting Keap1. *Oxid Med Cell Longevity*. 2021;2021:6688708-6688714.
135. Gorgulla C, Boeszoermenyi A, Wang ZF, et al. An open-source drug discovery platform enables ultra-large virtual screens. *Nature*. 2020;580(7805):663-668.
136. Kim S, Indu Viswanath AN, Park JH, et al. Nrf2 activator via interference of Nrf2-Keap1 interaction has antioxidant and anti-inflammatory properties in Parkinson's disease animal model. *Neuropharmacology*. 2020;167:107989.
137. Shimizu Y, Yonezawa T, Sakamoto J, Furuya T, Osawa M, Ikeda K. Identification of novel inhibitors of Keap1/Nrf2 by a promising method combining protein-protein interaction-oriented library and machine learning. *Sci Rep*. 2021;11(1):7420.
138. Li G, Liu H, Feng R, et al. A bioactive ligand-conjugated iridium(III) metal-based complex as a Keap1-Nrf2 protein-protein interaction inhibitor against acetaminophen-induced acute liver injury. *Redox Biol*. 2021;48:102129.
139. Zhang Y, Shi Z, Zhou Y, Xiao Q, Wang H, Peng Y. Emerging substrate proteins of Kelch-like ECH associated protein 1 (Keap1) and potential challenges for the development of small-molecule inhibitors of the Keap1-nuclear factor erythroid 2-related factor 2 (Nrf2) protein-protein interaction. *J Med Chem*. 2020;63(15):7986-8002.
140. Kopacz A, Kloska D, Forman HJ, Jozkowicz A, Grochot-Przeczek A. Beyond repression of Nrf2: an update on Keap1. *Free Radic Biol Med*. 2020;157:63-74.
141. Yoshida E, Suzuki T, Morita M, et al. Hyperactivation of Nrf2 leads to hypoplasia of bone in vivo. *Genes Cells*. 2018;23(5):386-392.
142. Noel S, Arend LJ, Bandapalle S, Reddy SP, Rabb H. Kidney epithelium specific deletion of kelch-like ECH-associated protein 1 (Keap1) causes hydronephrosis in mice. *BMC Nephrol*. 2016;17(1):110.

143. Wakabayashi N, Itoh K, Wakabayashi J, et al. Keap1-null mutation leads to postnatal lethality due to constitutive Nrf2 activation. *Nat Genet.* 2003;35(3):238-245.
144. Tsakiri EN, Gumeni S, Iliaki KK, et al. Hyperactivation of Nrf2 increases stress tolerance at the cost of aging acceleration due to metabolic deregulation. *Aging cell.* 2019;18(1):e12845.

AUTHOR BIOGRAPHIES

Enrique Crisman completed his BSc in Biotechnology at the University of Oviedo and his MSc in Drug Discovery at the University San Pablo CEU, University Complutense of Madrid and University of Alcalá de Henares. Currently, Enrique Crisman is enrolled in the Medicinal Chemistry PhD program at the University Complutense of Madrid. His research work is focused on the development of new multitarget-directed ligands combining NRF2 induction with additional activities for the treatment of Alzheimer's disease.

Pablo Duarte completed his BSc in Biotechnology at the University of Oviedo, and his MSc in Pharmacology Research at the Universidad Autónoma de Madrid. He is currently involved in a Pharmacology and Physiology PhD program at the Universidad Autónoma de Madrid. His research is focused on the discovery of new NRF2 inducers with complementary activities for the treatment of Parkinson's disease.

Esteban Dauden is a Full Professor in Dermatology at the Universidad Autónoma de Madrid, as well as Chief of the Department of Dermatology at the Hospital Universitario de la Princesa, Madrid (Spain). He graduated in Medicine at the Universidad Complutense de Madrid, and in 1993, he received his PhD at the same University. His research expertise is focused on immunoregulatory molecules as biomarkers, and the study of the gene expression profile in patients with Immune-mediated inflammatory diseases.

Antonio Cuadrado, is full professor of Biochemistry and Molecular Biology at the Department of Biochemistry, Medical School, Autonomous University of Madrid. His main interest is the validation of transcription factor NRF2, master regulator of cellular homeostasis, as a new therapeutic target in neurodegenerative disease.

María Isabel Rodríguez-Franco, PhD, is a Scientific Researcher at the Medicinal Chemistry Institute (CSIC, Spain). She leads several drug discovery projects in the field of neurological pathologies, including Alzheimer's disease. One of her current projects is focused on the discovery of new nonelectrophilic inhibitors of the protein-protein interactions between KEAP1 and NRF2.

Manuela G. Lopez, MD, PhD, and full professor of Pharmacology at the School of Medicine in the Autonomous University of Madrid (UAM). She is currently the Director of the Institute Teofilo Hernando for R&D of drugs-UAM and head of the NeuroDiscovery-NDD group. Her research interests focus on the identification of targets that regulate oxidative stress, neuroinflammation, and autophagy for the development of innovative treatments for neurodegenerative diseases.

Rafael León, PhD, and Full Scientist at the Medicinal Chemistry Institute (CSIC, Spain). His research interest is focus in the development of innovative multitarget drugs toward chronic complex diseases. Activity combinations are designed using the NRF2-ARE phase II antioxidant response as the main target combined with specific pathological pathways of different diseases including Alzheimer's, Parkinson's, and Multiple sclerosis.

SUPPORTING INFORMATION

Additional supporting information can be found online in the Supporting Information section at the end of this article.

How to cite this article: Crisman E, Duarte P, Dauden E, et al. KEAP1-NRF2 protein–protein interaction inhibitors: Design, pharmacological properties and therapeutic potential. *Med Res Rev.* 2023;43:237-287. doi:10.1002/med.21925